COMPARATIVE STRAIN ANALYSES IN A WELDED IGNIMBRITE: AN

ASSESSMENT OF WELDING INTENSITY VARIABLES AND RANKINGS

By

Roger Wesley Ward B.S.

A Thesis Submitted to the Department of Geological Sciences
California State University, Bakersfield
In Partial Fulfillment for the Degree of Masters of Science in Geology

Fall 2014

# COMPARATIVE STRAIN ANALYSES IN A WELDED IGNIMBRITE: AN ASSESSMENT OF WELDING INTENSITY VARIABLES AND RANKINGS

Roger Wesley Ward

The supervisory committee has accepted this thesis on behalf of the Department of Geological Sciences.

Graham Andrews, PhD., Chair
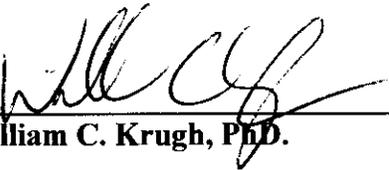
William C. Krugh, PhD.
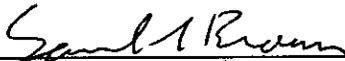
Sarah Brown, PhD.

Acknowledgements

I would like to express my appreciation to Dr. Graham Andrews for his insightful advice, mentorship, and encouragement throughout the duration of this project. His guidance and support has been essential in bringing this paper to fruition. This thesis has also benefited from the thoughtful input of Dr. Chris Krugh and Dr. Sarah Brown. I am very grateful to Elizabeth Powers for her help in the nuts and bolts of this project, and to William (Bill) Whitaker, Zachary Martindale, and Phil LaMothe for their assistance in porosity sample preparation. I am also thankful to Terry Pavlis and Darrel Cowan for the use of the SHEAR facilities during field work stages of this project. I am also very grateful to my parents Andrew and Deborah Ward for their endless encouragement and support through the entirety of this project. Lastly, I would like to thank my wife Heather for her many hours of assistance in the field as well as her continued patience over the last two and a half years. Funding for this project was provided by the Chevron Graduate Student Research Grant, Center for Research Excellence in Science and Technology (CREST) NSF award #1137774, and the Claude Fiddler Grant.

Abstract

Welding is the plastic deformation of pyroclastic material in response to high post-emplacement temperatures, load stresses, and to a lesser extent, retained volatile content. There are few field studies pertaining to the use of physical properties in the quantification of strain in welded ignimbrites, and even fewer that are contemporaneous with modern thermo-mechanical modeling of silicates. Accordingly, this study is a review of several methods for measuring strain in welded ignimbrites applied to the same deposit. The Resting Springs Pass tuff provides an excellent case-study for understanding the distribution of strain in welded ignimbrites. First-order petrofabric (strain measurements at different scales [field and thin section]) and petrophysical data (porosity) were collected to map the vertical distribution of strain throughout a single deposit and to assess the qualities of each of the data-sets and the strength of correlations between them

Accurate measurement of strain in the field and laboratory, while possible, is shown to be met with many practical challenges. Results from this study confirm the validity of using pumice clasts in a two-dimensional strain analysis. Volume strain and shear strain measurements are shown to be positively and well-correlated for much of the RSPT and presumably for similarly moderately welded ignimbrites. Only in the most strained, lowest porosity zone is there a significant difference between volume and shear strain: this zone is a black rheomorphic vitrophyre that suggests a different welding history from the rest of the RSPT.

Comparative Strain Analyses in a Welded Ignimbrite: an Assessment of Welding Intensity Variables and Rankings

Roger Ward

Introduction

Volcanic deposits exhibit an incredible range of lithofacies and corresponding variations in physical properties, even over small length-scales. One of the most important variations is in *welding intensity*; welding strongly influences porosity, permeability, mechanical strength, and preservation potential. Studies of welding have been sporadic over fifty years, initially emphasizing deposit characteristics (e.g., Smith, 1960a; Peterson, 1979) and evolving to quantitative modeling of welding rates (e.g., Quane and Russell 2005a; 2005b). However, there is still a basic lack of agreement about how to *measure* welding intensity in real deposits, and how to use these measurements in conjunction with quantitative experimental data to reconstruct the welding process (intensive parameters, time scales) in specific deposits. This study applies different, common techniques to investigate changes in welding intensity within a single unit.

Pyroclastic rocks are formed as a result of explosive fragmentation of silicic magma during a volcanic eruption. During fragmentation, liquid magma containing dispersed gas bubbles (bubbly magma) is transformed into a continuous gas phase with dispersed liquid or solid particles. As volatiles exsolve, the bubbly magma decreases in density and rises buoyantly, accelerating rapidly. Fragmentation of magma occurs when the shear stress on the magma exceeds its tensile strength. Pyroclastic rocks are composed of pumice and ash fragments. Avalanches of pyroclastic debris are called pyroclastic density currents (PDCs). PDCs can be categorized into either of two end-member categories: surges and flows. Pyroclastic surges are

fast (10-300 m/s), generally devoid of solids (0.1-1%), density stratified, and transport material primarily by means of turbulent suspension. Pyroclastic flows are generally slower (tens of meters per second), have higher percentages of solid content (high particle concentration), and transport material via turbulent particle-particle impact, and fluidization (Wilson and Houghton, 2000). The deposit of a PDC is an ignimbrite.

Ignimbrites

Ignimbrites are ubiquitous on the surface of the Earth; well-known ignimbrites in western North America include the Bishop Tuff (California, USA), the Bandelier Tuff (New Mexico, USA), the Rattlesnake Tuff, (Oregon, USA), and the tuff of the Valley of Ten Thousand Smokes (Alaska, USA). Because PDCs are gravity-driven and follow topographic lows, ignimbrite geometry is therefore, largely controlled by underlying topography. Nevertheless, ignimbrite geometry is generally highly variable with run-out distances ranging from a few hundred meters to 200 km, areal extents ranging from 100 m^2 to 45,000 km^2 (Ross and Smith, 1961), and volumes ranging between a few thousand cubic meters to about 5,000 km^3 (Freundt et al., 2000).

A typical ignimbrite is defined by Sparks et al. (1973) as consisting of a single flow unit (composed of two distinct layers) and two bounding deposits intimately associated with the single flow unit as products of the same eruptive event (Fig. 1). Layer 1 in a typical flow unit is a fine-grained, cross-bedded basal layer which ranges in thickness from a few centimeters to more than a meter. This is typically inferred to be the "surge-like" low particle concentration "head" of the PDC. Layer 2A is a laterally discontinuous, thin, fine-grained layer devoid of lapilli-sized (>2 mm) pyroclasts. Its origin and significance remain disputed (Branney and Kokelaar, 2002). Layer 2B of a typical ignimbrite flow unit constitutes the bulk of the deposit and is relatively homogenous, massive, poorly sorted, and typically normally graded with respect to lithic

4

fragments and reverse graded with respect to pumice clasts. Layer 2B is typically interpreted as the deposit of the high particle concentration "core" of the pyroclastic flow. Whether it is a laminar or turbulent flow regime has driven PDC research for the past 20 years (Branney and Kokelaar, 1992; 2002). Layer 3 is an overlying fine ash deposit which is created by the deposition of fine dust sourced from either the eruptive cloud or elutriated from the pyroclastic flow.

Branney and Kokelaar (1992, 1997, 2002) have shown that massively-bedded ignimbrites are deposited gradually by a sustained, quasi-steady, turbulent current, much like a submarine turbidity current (Fig. 2). This "progressive aggradation" model stands in stark contrast to previous models from Sparks et al. (1973) and Wright and Walker (1981) which cite *en masse* emplacement of ignimbrites as laminar-flowing slurries.

Welding in pyroclastic deposits

Ignimbrites are largely composed of silicic volcanic glass in the form of juvenile pyroclastic material (i.e. pumice and ash) that deform plastically at or close to magmatic temperatures (i.e. >600°C; Riehle, 1973). Welding is the process of plastic deformation of pyroclastic material in ignimbrites in response to high post-emplacement temperatures, load stresses, and to a lesser extent, retained volatiles (Smith, 1960a; Freundt et al., 2000, Grunder and Russell, 2005). As illustrated by Branney and Kokelaar (1992), the degree to which an ignimbrite can be welded is variable and is best represented as a continuum where higher emplacement temperatures, greater compaction, and higher water content all result in higher grades of welding (Fig. 3). Ignimbrites may become so densely welded that remobilization of material under a laminar flow regime occurs in a process called rheomorphism. In ignimbrites, welding is manifested as porosity loss and corresponding densification, and the development of a

planar fabric known as a eutaxitic foliation (e.g., Fig. 4). This eutaxitic foliation is marked by the parallel alignment of originally platy materials and the compaction of glass shards and pumice fragments into more oblate shapes, forming a penetrative foliation. The recognition of a eutaxitic foliation is often aided by the conspicuous presence of dense glassy lenses known as fiamme (Fig. 4). Fiamme are oriented in the plane of foliation (i.e. perpendicular to σ_1) and form as a result of the progressive flattening of originally more equant pumice clasts. One can track absolute changes in the degree of welding within an ignimbrite by measuring the deformation of features such as pumice clasts or vesicles (e.g., Peterson, 1979) and the spatial distribution of properties such as porosity and density (Sheridan and Ragan, 1976), then converting them into corresponding values of strain.

Strain in ignimbrites

Strain is the measure of the finite deformation an object experiences, and is typically measured by estimating the change in shape of an object from its original shape. During welding, ignimbrite deposits are vertically shortened (compacted) with respect to original deposit thickness in a combination of two ways: volume strain and shear strain. Volume strain is achieved by a progressive loss of porosity and corresponding densification (Fig. 5). Previous studies (e.g. Smith and Bailey, 1966; Ragan and Sheridan, 1972; 1976; Quane and Russell, 2004a; Russell and Quane, 2004) have used porosity and density to create compaction profiles which serve as a proxy for volume strain at varying heights within an ignimbrite.

Welding in ignimbrites also causes deformation in the form of coaxial (pure) shear strain. The amount of finite strain at any location within an ignimbrite can be determined by the change in relative lengths of the principle axes of the finite strain ellipse (Fig. 6). Ragan and Sheridan (1972) explored and confirmed the validity of using deformed shapes of bubbles and three-

6

pronged ash shards to obtain strain values. Peterson (1979) measured the flattening ratios in pumice clasts to elucidate the distribution of strain at different stratigraphic levels within the Apache Leap Tuff and concluded that in light of the variety of primary and secondary processes that can affect porosity, and the predictive ability of strain data from pumice clasts, strain data from pumice clasts was superior in the interpretation of cooling histories of ignimbrites.

This study

There are few field studies pertaining to the use of physical properties in the quantification of strain in welded ignimbrites, and even fewer that are contemporaneous with modern thermo-mechanical modeling of silicates. Accordingly, this study is a review of several methods for measuring strain in welded ignimbrites applied to the same deposit. The goal of this study is to use first-order petrofabric (strain measurements at different spatial scales [field and thin section]) and petrophysical data (porosity) to map the vertical distribution of strain throughout a single ignimbrite and to assess the qualities of each of the data-sets and the strength of correlations between them. The physical properties of ignimbrites such as the Resting Springs Pass tuff (RSPT) are highly variable and therefore present challenges in the practical aspect of data collection. Results from this study indicate that strain is partitioned unequally between matrix and clasts, and heterogeneously through the unit. Furthermore the nature of porosity is complex and studies quantifying welding by density-porosity only are of questionable use in some cases.

The Resting Springs Pass tuff

The Resting Springs Pass tuff (RSPT) is a 9.7 Ma, rhyolitic, welded ignimbrite located approximately 4 miles (6.4 km.) east of Shoshone, CA (Fig. 7; Heydari 1981) that covers an area of approximately 5.6 km^2. The RSPT was chosen for this study for several reasons: (1) it

contains all the features generally ascribed to a classic welded ignimbrite; (2) it is excellently exposed in a roadcut along Charles Brown Highway (State Highway 178); and (3) it is a famous geo-tourism spot between Death Valley and Las Vegas (Fig. 7). Previous to this study, Heydari (1981) and Troxel and Heydari (1982) have been the only significant investigations of the RSPT. Heydari (1981) provided a map, detailed petrologic descriptions, and a basic conceptual model for the emplacement of the RSPT in the Shoshone area. Troxel and Heydari (1982) investigated the RSPT where it is exposed in the roadcut along Hwy 178, proposing a sequence of events responsible for the creation of the visible features.

According to Troxel and Heydari (1982), the sequence of events responsible for the generation of the features seen in the Resting Springs Pass began with deposition of the Bonanza King Dolomite in the Cambrian (Hazzard, 1938). Cenozoic Basin and Range extension cut the Bonanza King Formation into east and west fault blocks to form the Resting Springs Range. Following a period of erosion, several ash flow and ash fall tuff deposits, sandstone and siltstone deposits, and one megabreccia deposit were formed in a basin adjacent to the Resting Springs Range. These beds were then cut by several normal faults shortly before the deposition of the Resting Springs Pass tuff which was emplaced at 9.7 Ma.

As stated by Troxel and Heydari (1982) "A specialist in volcanology will appreciate the quality of data available in a single cooling unit [the RSPT]". Given its superb exposure and impressive appearance, it is surprising that other studies are not published.

The Resting Springs Range is an eastward-dipping fault block composed of Cambrian strata and overlying Cenozoic volcanic cover. Resting Springs Pass cuts northwest-southeast through the Resting Springs Range, exposing the Cambrian Bonanza King Formation, Cenozoic Chicago Valley Formation, Gerstley Lake beds, and a single ignimbrite (Heydari, 1986). The

base of the RSPT is exposed in the roadcut along Hwy 178 and can be seen onlapping and overstepping a paleo-fault scarp in the faulted tuffaceous Gerstley Lake beds (Fig. 8). While the RSPT appears to be a compound cooling unit measuring up to 244 m thick in its westernmost exposure (Heydari, 1981), it outcrops as a simple cooling unit measuring between 60-200 ft. thick in its easternmost exposures (Heydari, 1986). Heydari (1981) divided the RSPT into five zones: the Lower Zone of No Welding, the Lower Zone of Partial Welding, the Zone of Dense Welding, the Upper Zone of Partial Welding, and the Upper zone of No Welding. The ignimbrite exposed in the roadcut contains the lowermost three of the five zones.

For the purposes of this study, the RSPT is informally divided into three zones: zone A, zone B, and zone C (Fig. 8). Zone A includes all the material from the base of the deposit up to the vitrophyre zone (zone B) and is characterized as grey to brown, non-welded to densely welded, being poorly sorted, clast-supported, with lapilli-sized pumice and lithic clasts in an ash matrix (Fig. 9, A+B). Zone A grades into a dark glassy vitrophyre zone denoted here as zone B (Fig. 9, C). The vitrophyre is perlitized, extremely brittle, and contains elongate vesicles partially filled by minerals including quartz, cristobalite, tridymite, and feldspar (Heydari, 1981). The transition between the vitrophyre (zone B) and the material above (zone C) is sharper and significantly less regular than the basal contact. Zone C includes all the material from the top of the vitrophyre to the eroded surface and is orange to light purple, densely welded, and contains abundant macroscopic voids (lithophysal cavities) ranging from 1-8 cm in diameter (Fig. 9, D+E). Zone C is likely eutaxitic; however, devitrification and lithophysal cavity development obscures nearly all original clast or grain morphologies.

Methods

This study investigates the distribution of strain within a single cooling unit by comparing various petrofabric and petrophysical data sets obtained in the field and laboratory. Six semi-independent analyses were conducted and their results are presented here: two dimensional strain measurements of clasts, groundmass, and voids, respectively; three dimensional strain measurements of clasts and voids; and porosity as a proxy for bulk strain.

Two-dimensional strain in pumice clasts and void spaces

As described in Sheridan and Ragan (1975), the two-dimensional state of finite strain at a point can be completely defined by the values and orientation of the two mutually perpendicular principal axes (Fig. 6). Therefore, the axial ratios of strain markers (pumice clasts and ash shards) were measured in outcrop and in thin section. When using the axial ratios of a given strain marker to conduct a two-dimensional strain analysis, it is necessary to know the original shape of the strain marker before deformation. While it is unlikely that any one pumice clast was perfectly spherical upon deposition, validity depends on the assumption that the average original shape was pseudo-spherical for a large number of pumice clasts. This can be assessed with reference to the non-welded portion of the deposit. In a similar fashion, ash shards, while grossly variable in original shape at the time of deposition, average a roughly triangular initial shape that conforms to a uniform shape during the welding process.

While pumice clasts or fiamme are observed throughout the entire height of the RSPT, their boundaries are only easily distinguishable in zone A (Fig. 9A, 9B); the clasts in this zone are readily visible and show a steadily increasing degree of apparent flattening upwards towards zone B. Zone A was measured and divided into nine one meter-thick thick sections and thirty pumice clasts were measured in each section. The number of measurements to make per section

10

was decided based on an effort to balance statistical viability and what would be easily gatherable in the outcrop. Using a digital micrometer, the longest axis (L_{max}) of each clast was measured first, parallel to the eutaxitic fabric where present, followed by the shortest axis (L_{min}) perpendicular to L_{max}. These length measurements were taken without discrimination of size or shape. Natural strain ($\bar{\varepsilon}$) is calculated thus:

$$\bar{\varepsilon} = ln\left(\left(\frac{L_{min}-L_o}{L_o}\right) + 1\right)$$

(1)

Where the original clast diameter (L_0) is given by:

$$L_0 = \sqrt{L_{max} \times L_{min}}$$

(2)

Macroscopic void spaces are completely absent in zone A; however, they are common in zones B and C. Together, these zones were divided up into eleven one meter-thick sections and thirty void spaces were measured in each of the eleven sections. The axial ratios of the void spaces were measured and calculated in exactly the same way as the pumice and fiamme clasts.

Two-dimensional strain in the groundmass

Eight hand samples were collected from the RSPT, each from a different height within the deposit (Fig. 10). One thin section was made from each of the samples collected (Fig. 11). Due to the intensity of micro-fractures found throughout the vitrophyre (zone B) and the friability of the non-welded ignimbrite at the base (zone A), thin sections could not be prepared for those zones.

Using a digital camera mounted on a Nikon E200 petrographic microscope, ten photomicrographs were taken of each thin section under plane-polarized light. Special care was taken to ensure that there was no overlap of thin section in any of the photos. Photographs were taken at x2 or x4 magnification depending on the size of the ash shards in thin section. Each thin

section was examined under cross polarized light and any crystal content was carefully noted to avoid mistaking crystals for ash shards. The photographs were printed and the axial ratios of ten ash shards were measured on each photo. Ash shards were chosen primarily on the clarity of their boundaries and without respect to inferred original shape. A ruler with millimeter and centimeter divisions was used to measure the longest (L_{max}) and shortest (L_{min}) perpendicular axis of each selected ash shard (Fig. 11). The natural strains from each thin section were then calculated.

Three-dimensional strain data in voids

Unlike two-dimensional data, three-dimensional strain data can reveal the strain ellipsoid of a deformed body and qualify the relative proportions of flattening and stretching along mutually perpendicular axes. Understanding the relative proportions of flattening vs. stretching is key to delineating the presence of coaxial vs. non-coaxial shear strain. Undergraduate and graduate students in an Advanced Structural Geology class collected three-dimensional strain ellipse data (maximum and minimum axes) on voids in zones B and C where exposed in mutually perpendicular vertical planes, one (XZ) parallel to the principal elongation direction (X) and one perpendicular to X (YZ). These data are combined to represent the three-dimensional strain ellipsoids in graphical plots: Flinn and Hsu diagrams.

The Flinn diagram plots the XY and YZ axial ratios to define oblate (flattening-dominated) and prolate (stretching-dominated) fields separated by a line of "plane strain" (X>Y=1>Z), the regime typical of most ductile shear zones. Oblate fabrics are pancake-shaped, prolate fabrics are cigar-shaped, and plane strain is intermediate (surfboard-shaped). Plane strain has a *k*-value of 1, where

$$k = \tan q \qquad (3)$$

where q is the slope of a line passing through the origin (1,1). Oblate fabrics have k-values

between 0 and 1; prolate fabrics have k-values between 1 and infinity.

The Flinn diagram plotting parameters are:

for the abscissa:

$$R_{yz} = (1+Y)/(1+Z) \qquad (4)$$

for the ordinate:

$$R_{xy} = (1+X)/(1+Y) \qquad (5)$$

where:

$$k = (R_{xy} - 1) / (R_{yz} - 1) \qquad (6)$$

When data is collected in the XZ plane, the following translation is required:

$$R_{xy} = R_{xz}/R_{yz} \qquad (7)$$

The Flinn diagram is excellent at quantifying shape fabrics but does not take fabric orientation

into account, i.e. coaxial (layer parallel) and non-coaxial (layer oblique) shear strains are

indistinguishable. More importantly for this study, the Flinn diagram does not quantify total

strain. Intuitively the distance away from the origin (1,1) is related to total strain but this

relationship is not equal across fields such that total strains between oblate and prolate end-

members are not comparable.

The Hsu diagram is used to successfully quantify shape fabric and total strain where the dimensionless natural octahedral unit shear strain ($\bar{e}_s$) and Lode parameter (v) are plotted (Fossen, 2010). The Lode parameter is derived thus:

$$v = \frac{2\bar{e}_Y - \bar{e}_X - \bar{e}_Z}{\bar{e}_X - \bar{e}_Z} \tag{8}$$

where $\bar{e}_n$ is the natural strain for one of the three principal strains (X, Y, and Z).

The natural octahedral unit shear strain is calculated thus:

$$\bar{e}_s = \sqrt{3}/2 \times \bar{\gamma}_{oct} \tag{9}$$

where $\bar{\gamma}_{oct}$ is:

$$\bar{\gamma}_{oct} = 2/3 \times \sqrt{(\bar{e}_X - \bar{e}_Y)^2 + (\bar{e}_Y - \bar{e}_Z)^2 + (\bar{e}_Z - \bar{e}_X)^2} \tag{10}$$

The Hsu diagram allows direct comparison of the total strain, expressed as $\bar{e}_s$, for all shape fabrics on a scale of 0 (spherical) to 3 (infinity). The Lode parameter varies from -1 (pure prolate) to 1 (pure oblate); plane strain equals zero.

Porosity

Fifteen bulk samples (A-P) were collected from various heights within the RSPT (Fig. 12). Because each sample displayed vastly different levels of competency due to varied degrees of welding, several different methods of sample preparation were employed to obtain the porosity values desired. For eleven of the fifteen samples, a drill press fitted with a water-cooled coring bit was used to core the bulk samples. The 1" diameter (2.54mm) cores were trimmed to a cylindrical shape with a water-cooled rock saw and left to dry in an oven for 24 hours. Using a

pair of digital calipers, five diameter measurements and five length measurements were collected

and averaged together to obtain representative values for each core sample. From these values,

bulk volume (V_B) was calculated.

Sample N is only incipiently welded and was therefore too fragile to be cut with a wet

saw and was instead trimmed with a wood saw and sanded into the shape of a cuboid. Sample I

is densely welded but fractured easily during coring, therefore, it was reinforced with duct tape

and cut into a cuboid shape with a rock saw.

The remaining two samples (O and P) from the lower non-welded part of the RSPT were

too fragile to core and were therefore gently crumbled by hand instead. Crumbled samples O and

P were then poured into a graduated cylinder to measure their bulk volume. The graduated

cylinder was vibrated gently before measurement to allow settling of material and to minimize

air pockets.

The porosity of these core samples was measured using a Quantachrome

Multipycnometer (Fig. 13). Samples were weighed on a balance, placed in the multipycnometer,

purged of air, and then measured for skeletal porosity (Φ_S) by helium displacement. Skeletal

porosity was divided by bulk volume to get a connected porosity value (Φ_C) (eq. 11), the portion

of the porosity with high affective permeability:

$$\Phi_c = 1 - \left(\frac{\Phi_S}{v_B}\right) \tag{11}$$

Bulk density (ρ_b) was calculated thus:

$$\rho_b = \frac{M}{V_B} \tag{12}$$

$$\rho_r = \frac{M}{\left(V_B - (V_B \times \Phi_s)\right)} \tag{13}$$

Volume strain

Deformation (i.e. strain) due to loss of porosity can be quantified as volume strain (e_φ; Quane and Russell, 2005):

$$e_\varphi = \frac{(\varphi_O - \varphi_1)}{(1 - \varphi_1)} \tag{14}$$

where, φ_O is the inferred original porosity, typically assumed to be 60% (Sheridan and Ragan, 1976; Quane and Russell, 2005a) and φ_1 is the measured porosity of the sample. The assumed original porosity (60%) is reasonable for the RSPT where the maximum sustained values in the non-welded part of zone A are ~58%. Samples with negative values of volume strain are less porous, and therefore more compacted (i.e. compressively strained), than the non-welded, non-strained ignimbrite.

Results

Two-dimensional strain in clasts

Measurements of two-dimensional strain in clasts (pumice and fiamme) were limited to zone A because there are no readily visible clasts in any of the overlying deposit. The data from pumice and fiamme clasts in zone A show a remarkably smooth and gradual increase in strain from -0.13 to -0.94 from the base of the deposit to the middle of the deposit (Table 1, Fig. 14). The strain gradient increases upwards from -0.028/m (0 m - 5.7 m), to -0.14/m (5.7 m - 7.8 m), to -0.4/m (7.8 m – 9.0 m). This corresponds with the visual shape and color changes seen in the change of pumice into fiamme.

Two-dimensional strain in voids

Measurement of two-dimensional strain in macroscopic voids was limited to zones B and C because there were no macroscopic voids present in zone A. The data from the voids show a highly irregular but increasing trend in strain from zone B to about one third of the way up through zone C and steadily decreasing strain from there on to the top of the deposit (Table 1, Fig. 15). The strain gradient changes from -0.24/m (9-13 m) to 0.16/m (13-20 m); the change in strain gradient correlates with the visual estimate of shape change.

Two-dimensional strain in the groundmass

The four samples collected within Zone A (RH5-8; Fig. 16 A-D), especially samples RH5 and RH8, show generally unimodal Gaussian distributions and a close agreement between the mean, median, and modal values (Fig. 17). Samples RH8 and RH7 (2.7 m and 5 m above the base respectively) both show a low average natural strain value of -0.28. Sample RH6 (7.0 m

above the base) was sourced from about the same height that pumice deformation begins to accelerate and yielded a slightly higher natural strain value of -0.30. Sample RH5 (8.7 m above the base) has a high natural strain value of -0.94. Together, data from the ash groundmass shows that strain accumulation in individual ash shards increases only slightly from the base to 6.7 m (-0.003/m) whereupon it rapidly accelerates at 9.0 m towards the vitrophyre (-0.15/m; Table 1, Fig. 18). High-grade welding and devitrification of samples from above zone A (RH1-4) obscures individual ash shard boundaries, thereby making thin section analysis impossible in zones B and C (Fig. 16 E-H).

Three-dimensional strain in voids

When plotted on the Flinn and Hsu diagrams (Figs. 19, 20), the three-dimensional strain data from both zones B and C give average values that plot in the prolate field. On the Hsu diagram, the average total strain value for voids in zone B is ~1.8, which is ~0.8 greater than the average total strain value for voids in zone C.

Porosity

Table 2 contains volume, weight, density, and porosity data for the 15 samples collected. In zone A, samples J through P (Fig. 21, #2) show relatively high constant porosity values (~58%) with a strain gradient of -0.0/m from the base of the deposit to about 7 m where it begins to dramatically decrease (Fig. 21). Sample M shows an anomalously high value (80%) that is most likely attributable to an inaccurate bulk volume caused by the lack of sharp corners on the cube-shaped sample. The lowest porosity value (22%) comes from sample H which was taken from the very top of zone A. While There is a sharp increase in porosity in the 0.5 m above the

vitrophyre zone from ~20% to 40%. Zone C is characterized by unsteadily increasing and decreasing porosity (40% to 55% to 35%).

Volume strain

Zone A of the RSPT displays negligible, but constant volume strain (Fig. 21, #3) except where it approaches zone B. While no samples could be collected from zone B, strain in zone A increases significantly towards the base of zone B. It is logical to extrapolate this rapidly increasing trend in volume strain into zone B, because the vitrophyre has the lowest porosity when estimated visually. The trend of volume strain through zone C, while highly irregular, does display minimally decreasing strain values (-0.51 to -0.10); this probably reflects the heterogeneous distribution of anomalously large voids.

Discussion

Distribution of strain in the RSPT by correlating between the different data sets

Zone A

While no strain information could be gathered from the ash matrix or macroscopic voids in the base of zone A, pumice clasts indicated a slowly increasing strain gradient that accelerates from -0.13/m up to -0.4/m towards the base of zone C. The low strain value at the base of the deposit supports the assumption that the average shape of the pyroclasts before deformation is near equant (Fig. 14). Furthermore, the strong trend in strain averages supports the validity of using pumice clasts for measurement of strain in the field (Peterson, 1979).

Once the strain gradient in the pumice clasts reaches values in excess of -0.14/m, the low strain gradient in the ash matrix (Fig. 18) begins to increase appreciably from a near-zero value of -0.004/m. The relationship between these strain gradients indicates that load stress first results in volume strain of extremely porous pumice clasts until they reach porosities similar to the surrounding ash matrix (e.g., Quane and Russell, 2005a) whereupon volume strain and coaxial (pure) shear stress accumulate in the pumice and ash in relatively comparable rates. This interpretation is supported by generally constant porosity values in the lower half of zone A.

Zone B

Without a doubt, zone B is the most challenging zone to obtain strain data from. However, extrapolation of porosity and strain data trends from clasts and matrix into zone B are logical and are supported by the dramatic changes in color from buff to brown to black and in the coherence of the ash matrix. When extrapolated into zone B, trends in strain and porosity show this zone to be the most strained and to have the lowest porosity (Fig. 22). The drastic drop in

20

porosity near the zone A-zone B transition (as quantified by the change in strain gradient from 0.0 to -13.55(Fig. 21)) is likely due to the resorption of volatile gases trapped in pore spaces back into the glass (e.g., Sparks et al., 1999). The resorption of these gasses would serve to dramatically decrease the viscosity of the glassy material by several orders of magnitude, thereby creating a positive-feedback system within zone B. Once all gasses have been resorbed and porosity thereby effectively "destroyed", volume strain rapidly ceases and coaxial (pure) shear strain dominates.

Zone C

Concerning porosity in zone C, local variability can be attributed to the heterogeneous distribution of cavernous or "vuggy" pore spaces throughout the rock. This heterogeneous distribution of pore space may result in porosity samples that are not accurate representations of true porosity at their source locations, especially in the case of smaller samples. Additionally, these vesicles and cavities are products of secondary processes (i.e. volatile exsolution); therefore their porosity cannot be directly compared to porosity from zone A where all porosity is in the form of degraded primary porosity.

The correlation between porosity and strain from two-dimensional macroscopic void spaces in zone C is mixed (Fig. 22). While porosity is seen generally increasing with height through zone C, the two-dimensional strain gradients gathered from the macroscopic void spaces shows strain to initially increase until one third of the way through zone C before decreasing towards the top of the deposit.

Evidence for rheomorphism

When plotted on Flinn and Hsu diagrams (Fig. 19 and 20), three-dimensional data from vesicles in zone B plot in the prolate field, suggesting that there has been some level of rheomorphic flow in that zone (e.g., Schmincke and Swanson, 1967; Branney and Kokelaar, 1992; Andrews and Branney, 2011). By comparing two-dimensional and three-dimensional strain data, one can see that once volume strain ceases, coaxial shear accelerates from zone A into zone B and becomes overprinted by non-coaxial shear strain (prolate ellipsoids) caused by rheomorphism. Since the RSPT was deposited on a paleo-slope, any non-coaxial shear strain on account of rheomorphic flow would have been directed in a downslope direction.

The strengths and weaknesses of competing methods for measuring strain in welded pyroclastic deposits

The primary goal of this project is to assess the validity and application of competing methods of measuring strain in welded ignimbrites.

Sampling and sample material

Significant challenges exist in collecting accurate strain and porosity data from ignimbrites with physical properties that vary as widely as they do in the RSPT, such as porosity which ranges from 22% to >60%. Zone C contains cavities that are dispersed randomly throughout the deposit and can measure in excess of 15 cm in diameter; the challenge exists of obtaining a sample that will accurately represent the average pore space from that given location in the deposit. Accurate representations of volume strain from porosity are also retarded by the mineral infilling of pore spaces during diagenesis.

There is the additional ambiguity concerning the *nature* of porosity, specifically whether the pore space represents remnant original porosity or if it was created by secondary processes

(e.g., vesiculation). When collecting samples for porosity, it is necessary to obtain a sample with a geometric shape that allows for the calculation of bulk volume. Coring is feasible only where the deposit has sufficiently been crystalized (devitrified), such as in zone C, and yields the best results when the core bit is held securely such as in a drill press. Cutting cuboid-shaped samples with a rock saw or wood saw is superior to wet coring in zones like zone A where welding has not caused sufficient sintering of ash together. When collecting samples for porosity measurement, each sample must be treated uniquely according to the level of competency it shows. Problematic areas include the lower non-welded base of zone A where the ash disintegrates under the slightest pressure; the vitrophyre zone of zone B that is very intensely fractured; and at the base of zone C where various cavities and mineral infillings have created rock that behaves in an unpredictably brittle fashion.

The wide variation in rock coherence seen in the RSPT limits the use of thin sections in strain analysis. The ability to cut thin sections is limited to zones where welding has progressed enough to allow ash shards to sinter together; zone B of the RSPT is too fractured and microfractured to be make thin sections. Pervasive crystallization (devitrification) throughout zone C, such as can be seen in Figure 16F, has obscured any possible strain markers in the matrix, thereby making strain analysis of the matrix in this zone impossible.

Correlation between strain measurements

Each method of estimating strain applied to RSPT has positives, for example, ease of measurement and ability to collect large data-sets. However, the inability for any one strain measurement, with the exception of volume strain, to be used throughout the entire deposit is a major drawback. When correlated, all the methods together record a gradual increase in strain

with height from a minimum in zone A to a maximum in zone B, followed by a decrease towards the top of the preserved deposit (Fig. 23).

For volume strain, a derivative of porosity, to be a useful strain measurement it must be comparable and relatable to the measured longitudinal shear strain (i.e. shape change in strain markers). A simple correlation test (Fig. 24) shows that throughout most of the RSPT longitudinal strain and volume strain are positively ($y = 0.7x + 0.08$) and well-correlated ($r^2 = 0.67$). Only in zone B, the most intensely welded zone, is the relationship poorly correlated: volume strain is over three times greater than the measured longitudinal strain in the same horizon. Zone B is also the lowest porosity, most strained, only rheomorphic part (non-coaxial deformation and prolate shape fabrics), most different looking (black, clasts absent or obscured), and has the highest effective stress.

The RSPT data indicates that rapid, non-linear changes in physical properties occur within the deposit and are concentrated and maximized in a single discreet zone (zone B); this is similar to several other ignimbrites that experienced the onset of rheomorphism during or immediately following welding (e.g., Rattlesnake Tuff, Oregon [Streck and Grunder, 1995]). Is there something fundamentally different about zone B? One explanation worthy of further study is whether or not volatile resorption during welding and porosity-reduction (e.g., Sparks et al., 1999) drives the viscosity of zone B to lower values (at constant temperature), and thereby allows for accommodation of more strain, including lateral, non-coaxial shear strain (rheomorphic flow).

Summary

The RSPT provides an excellent case-study for understanding the distribution of strain in welded ignimbrites. Welding in ignimbrites is a complex process which causes different strain regimes in different locations. Three welding zones are distinguished: a lower zone (zone A) that becomes progressively more welded and strained upwards to a black glassy zone of maximum strain and minimum porosity (zone B), and an upper zone (zone C) that shows gradually reducing strain towards the top of the deposit. This architecture is typical of many welded ignimbrites.

Accurate measurement of strain in the field and laboratory, while possible, is met with many practical challenges, each requiring unique solutions and special considerations. Results from this study confirm the validity of using pumice clasts in a two-dimensional strain analysis (e.g., Peterson, 1979; Quane and Russell, 2005a). Obtaining a sample for the purpose of quantifying strain that is coherent, representative of its source, and reflective of primary vs. secondary porosity is difficult. However, for much of the RSPT and presumably for similarly moderately welded ignimbrites, volume strain and shear strain measurements are positively and well-correlated. Only in the most intensely welded zones are the volume and shear strain measurements not correlated; zones such as this are the most strained, among the most difficult to collect data from, and, in this case at least, rheomorphic.

References

Andrews, G.D.M., and Branney, M.J., 2011, Emplacement and rheomorphic deformation of a
    large, lava-like rhyolitic ignimbrite: Grey's Landing, southern Idaho: Geological Society
    of America Bulletin, v. 123, p. 725-743

Branney, M.J., and Kokelaar, P., 1992, A reappraisal of ignimbrite emplacement; progressive
    aggradation and changes from particulate to non-particulate flow during emplacement of
    high-grade ignimbrite: Bulletin of Volcanology, v. 54, p. 504-520.

Branney, M.J., and Kokelaar, P., 1997, Giant bed from a sustained catastrophic density current
    flowing over topography: Acatlán ignimbrite, Mexico: Geology, v. 25, p. 115-118.

Branney, M.J., and Kokelaar, P., 2002, Pyroclastic density currents and the sedimentation of
    ignimbrites. Geological Society of London, Memoirs 27. 152 pages.

Fossen, H., 2010, Structural Geology: New York, Cambridge University Press, 480 pages.

Freundt, A., Wilson, C.J.N., and Carey, S.N., 2000, Ignimbrites and block-and-ash flow deposits,
    in Sigurdsson, H., Houghton, B.F., McNutt, S.R., Rymer, H., and Stix, J., eds.,
    Encyclopedia of volcanoes: San Diego, California, Academic Press, 581-599 p.

Grunder, A., and Russell, J.K., 2005, Welding processes in volcanology: Insights from field,
    experimental, and modeling studies: Journal of Volcanology and Geothermal Research,
    v. 142, p. 1-9

Hazzard, J., 1938, Paleozoic section in the Nopah and Resting Springs Mountains, Inyo County,
    California: California Journal of Mines and Geology, v. 33, p. 273-339.

Heydari, E., 1986, Geology of the Resting Spring Pass Tuff, Inyo County, California: California

    Geology, v. 39, p. 253-261.

Peterson, D.W., 1979, Significance of the flattening of pumice fragments in ash-flow tuffs:

    Geological Society of America Special Paper 180, p. 195-204.

Quane, S.L., and Russell, J.K., 2005a, Ranking welding intensity in pyroclastic deposits: Bulletin

    of Volcanology, v. 67, p. 129-143, doi: 10.1007/s00445004-0367-5.

Quane, S.L., and Russell, J.K., 2005b, Welding: Insights from high temperature analogue

    experiments: Journal of Volcanology and Geothermal Research, v. 142, p. 67-87.

Ragan, D.M., and Sheridan, M.F., 1972, Compaction of the Bishop Tuff, California: Geological

    Society of America Bulletin, v. 83, p. 95-106.

Riehle, J.R., 1973, Calculated compaction profiles of rhyolitic ash-flow tuffs: Geological Society

    of America Bulletin, v. 84, p. 2193-2216.

Riehle, J.R., Miller, T.F., and Bailey, R.A., 1995, Cooling, degassing, and compaction of

    rhyolitic ash-flow tuffs: a computational model: Bulletin of Volcanology, v. 57, p. 319–

    336.

Ross, C.S., and Smith, R.L., 1961, Ash-Flow tuffs: Their origin, geologic relations and

    identification: U.S. Geological Survey Professional Paper 336.

Russell, J.K., and Quane, S.L., 2005, Rheology of welding: Inversion of field constraints: Journal

    of Volcanology and Geothermal Research, v. 142, p. 173-191.

Schmincke, H.-U., and Swanson, D.A., 1967, Laminar viscous flowage structures in ash-flow

    tuffs from Gran Canaria, Canary Islands: Journal of Geology, v. 75, p. 641-664.

Sheridan, M.F., and Ragan, D.M., 1976, Compaction of Ash-Flow Tuffs. *in* Chilingarian, G.V., and Wolf, K.H., eds., Compaction of Coarse-Grained Sediments, Elsevier, v. II., Amsterdam, Netherlands, p. 677-717.

Smith, R.L., 1960a, Ash-Flows: Geological Society of America Bulletin, v. 71, p. 795-842.

Smith, R.L., 1960b, Zones and zonal variations in welded ashflows: U.S. Geological Survey Professional Paper, 354-F, p. 149– 159.

Sparks, R.S.J., Self, S., and Walker, G.P.L., 1973, Products of ignimbrite eruptions: Geology, v. 1, p. 115-118.

Sparks, R.S.J., Tait, S.R., and Yanev, Y., 1999, Dense welding by volatile resorption: Journal of the Geological Society of London, v. 156, p. 217-225.

Streck, M.J., and Grunder, A.L., 1995, Crystallization and welding variations in a widespread ignimbrite sheet; the Rattlesnake Tuff, eastern Oregon, USA: Bulletin of Volcanology, v. 57, p. 151-169.

Troxel, B.W., and Heydari, E., 1982, Basin and Range geology in a roadcut, *in* Cooper, J.D., Troxel, B.M., and Wright, L.A., eds., Geology of Selected Areas in the San Bernardino Mountains, western Mojave Desert, and Southern Great Basin, California, Field trip number 9: Geological Society of America, Cordilleran Section Guidebook, p. 91-96.

Wright, J.V., and Walker, G.P.L., 1981, Eruption, transport and deposition of ignimbrite: a case study from Mexico: Journal of Volcanology and Geothermal Research, v. 9, p. 111-131.

Pumice Clasts			Macroscopic Voids			Matrix	
Height (m)	ε		Height (m)	ε		Height (m)	ε
0.67	-0.13		8.67	-0.39		2.67	-0.28
1.67	-0.11		9.73	-0.27		5.00	-0.28
2.67	-0.17		10.80	-1.04		7.00	-0.30
3.67	-0.22		11.80	-0.63		8.67	-0.56
4.67	-0.21		12.47	-1.32			
5.67	-0.27		13.80	-0.91			
6.67	-0.39		14.80	-1.10			
7.67	-0.54		15.80	-0.66			
8.67	-0.94		16.80	-0.54			
			17.80	-0.47			
			18.80	-0.32			

Table 1. Average two-dimensional natural strain values from pumice clasts, macroscopic voids, and matrix from the Resting Springs Pass Tuff. Values from pumice clasts macroscopic voids are averages of 30 values each and values from the matrix are averages of 100 values each.

Core	Weight (g)	Avg. V_s (cm^3)	Avg. Density (g/cm^3)	Radius (cm)	Length (cm)	V_b (cm^3)	Connected Porosity	Height (ft.)	Height (m)	V_{strain}
A	36.15	11.32	1.93	1.27	3.69	18.70	39.47	60	20.00	-0.53
B	33.81	10.41	1.89	1.27	3.55	17.92	41.91	56	18.67	-0.44
C	19.69	4.75	1.89	1.27	2.07	10.44	54.51	52	17.33	-0.10
D	29.99	8.88	1.62	1.27	3.66	18.48	51.95	48	16.00	-0.16
E	30.59	9.15	1.76	1.27	3.43	17.41	47.43	44	14.67	-0.27
F	35.16	11.44	2.06	1.27	3.39	17.05	32.89	40	13.33	-0.85
G	32.78	10.52	1.87	1.27	3.49	17.55	40.05	34	11.33	-0.51
H	34.55	11.67	2.30	1.27	2.97	15.02	22.31	26	8.67	-1.77
I	23.05	7.01	2.11	-	-	10.95	35.99	22	7.33	-0.69
J	16.08	3.73	1.79	1.27	1.79	9.00	58.49	18	6.00	-0.03
K	25.61	7.89	1.54	1.26	3.35	16.61	52.50	14	4.67	-0.15
L	23.83	7.19	1.39	1.26	3.45	17.15	58.11	10	3.33	-0.03
N	11.28	1.75	1.27	-	-	8.89	80.29	6	2.00	0.26
O	13.45	5.85	1.00	-	-	13.5	56.65	2	0.67	-0.06
P	11.8	5.15	0.94	-	-	12.5	58.82	0	0.00	-0.02

Table 2. Height, weight, volume, density, porosity, and strain data from the Resting Springs Pass tuff. Samples I, N, O, P do not have radius or length measurements because they were cubed or crushed.
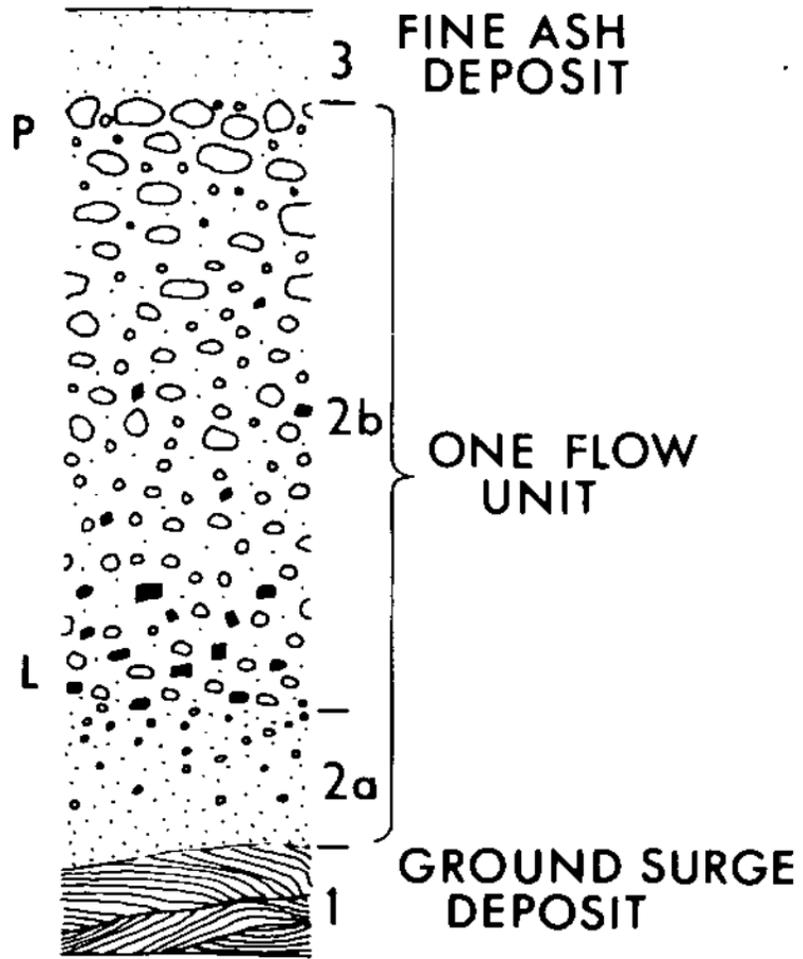
Figure 1. Typical architecture of a non-welded ignimbrite as defined by Sparks (1973). P = pumice clasts; L = lithic clasts.
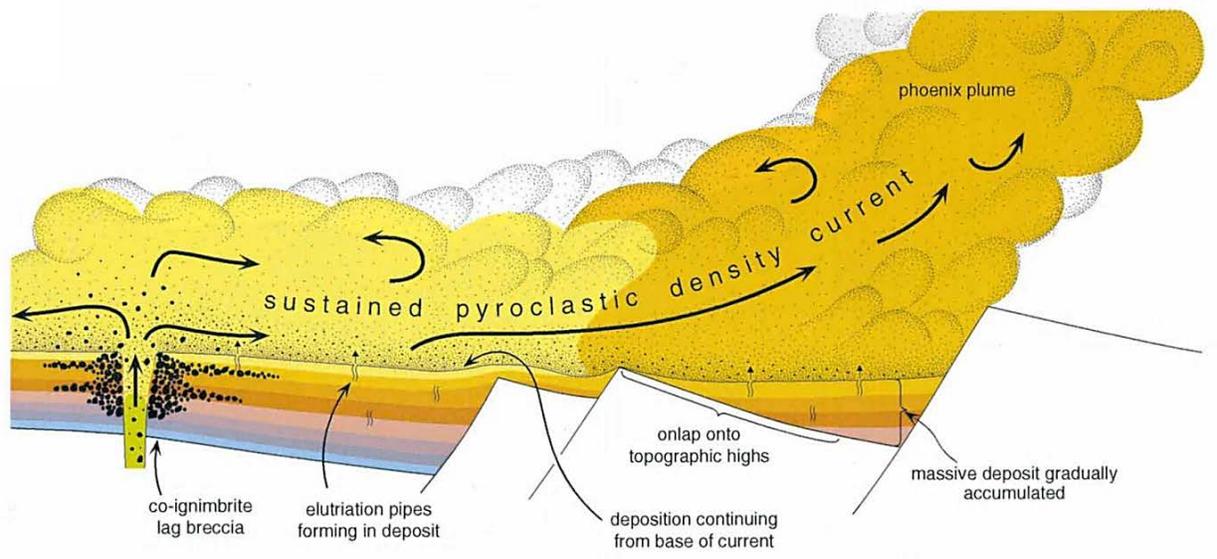
Figure 2. Progressive aggradation model for ignimbrite emplacement proposed by Branney and Kokelaar (1997).
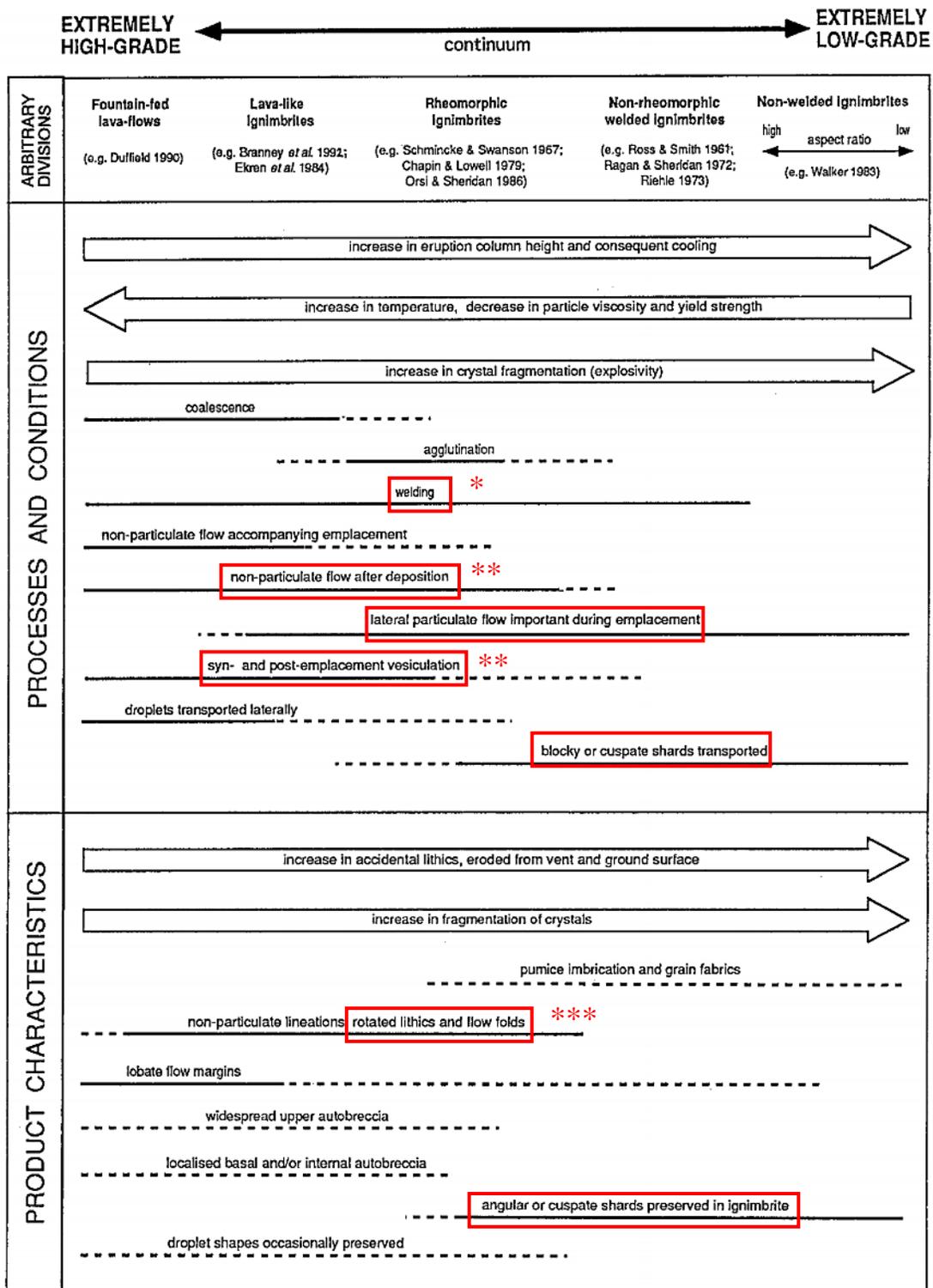
Figure 3. The ignimbrite grade continuum proposed by Branney and Kokelaar (1992). Processes, conditions, and characteristics observed in the Resting Springs Pass tuff are denoted with red boxes. *Occurs in all but base. **Restricted to the vitrophyre and material directly above the vitrophyre. ***Exclusive to the material directly above the vitrophyre.
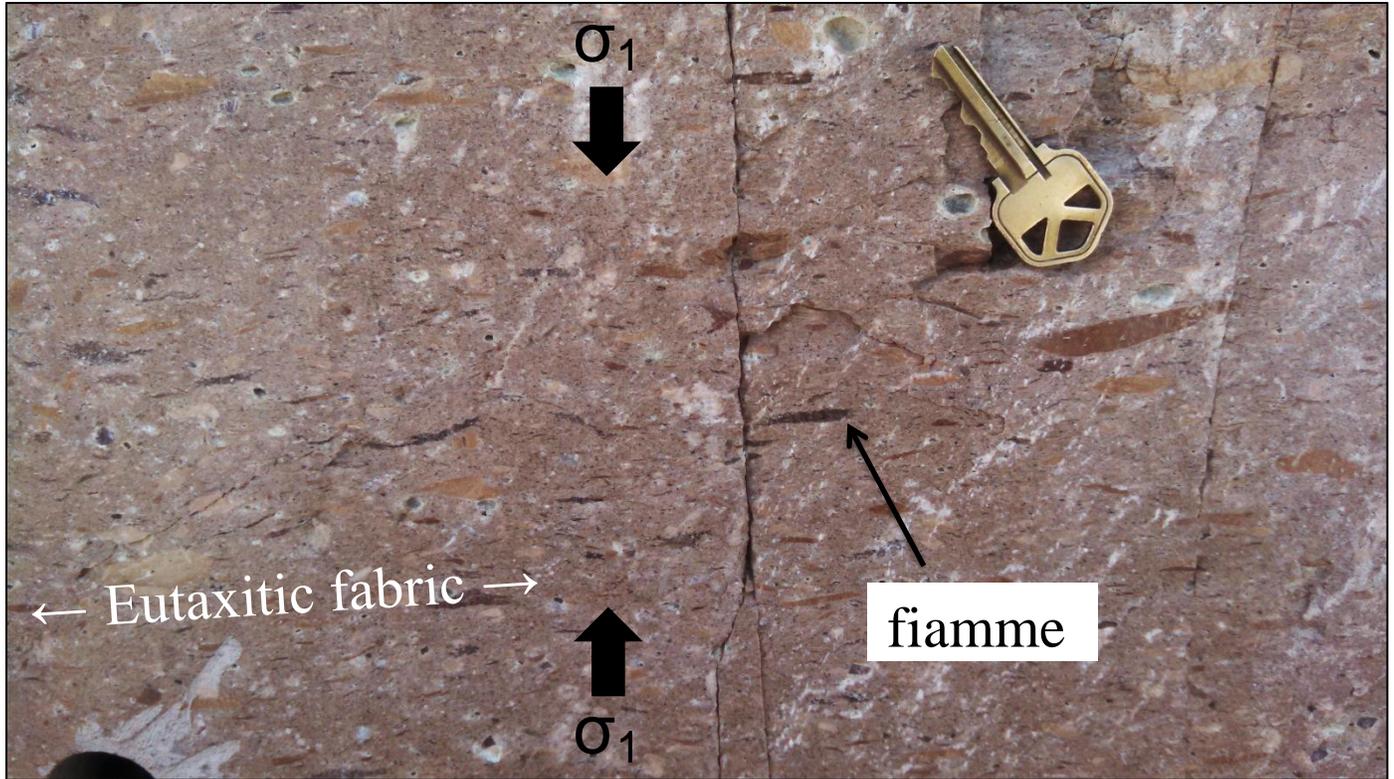
Figure 4. Eutaxitic texture seen in Zone A of the Resting Springs Pass tuff. The thin dark lenses that help define a plane of foliation are fiamme. Sigma 1 arrows indicate the direction of maximum stress and are interpreted from the maximum shortening direction of the fiamme. Key is 5.3 mm long.
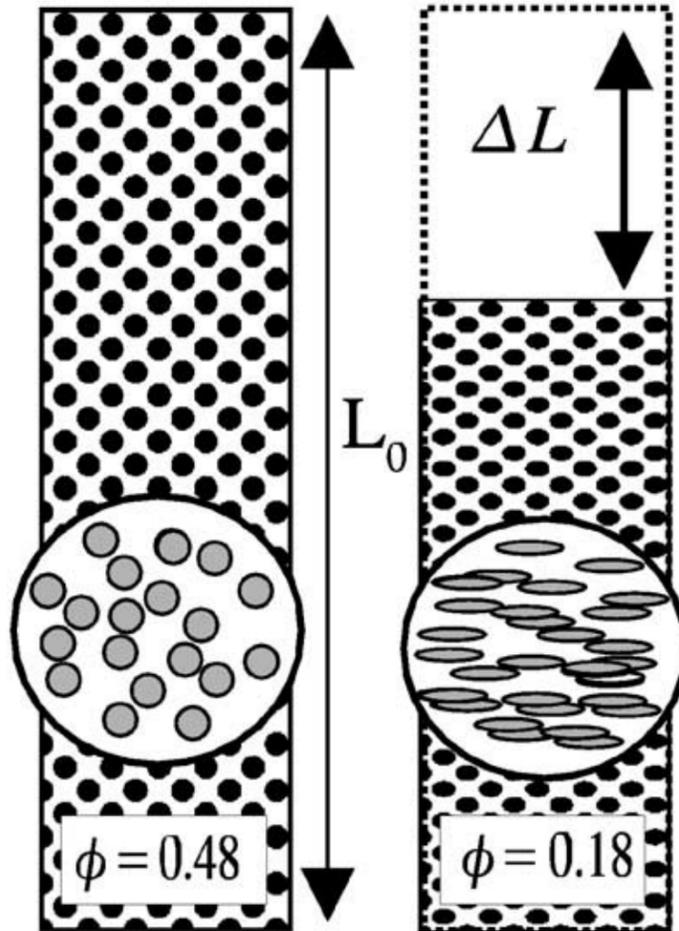
Figure 5. Schematic representation of volume strain in welded ignimbrites. Figure from Russell and Quane (2004). Lo = original deposit thickness; ΔL = amount of vertical shortening; Φ = porosity.
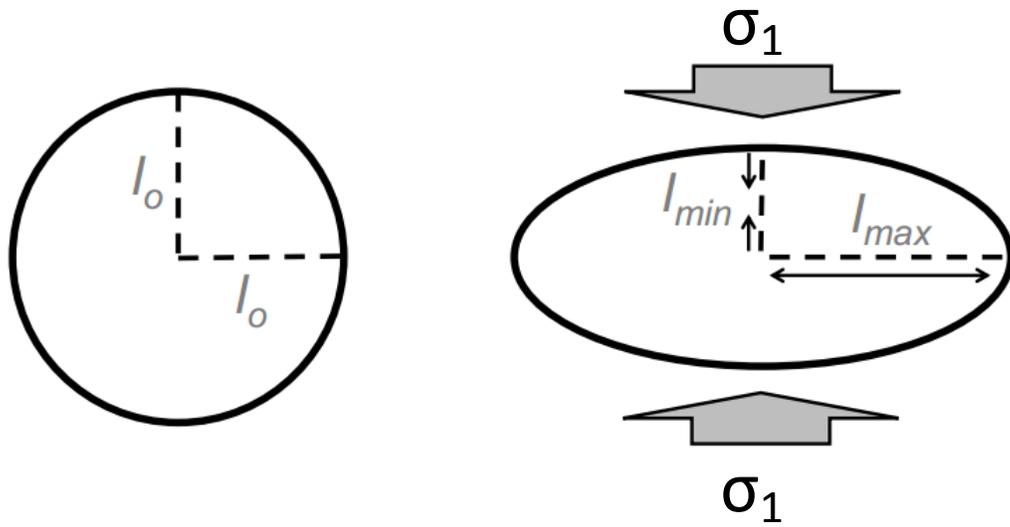
Figure 6. An illustration of the changes in the lengths of principle strain axes in response to a pure shear force exerted on an originally spherical shape.
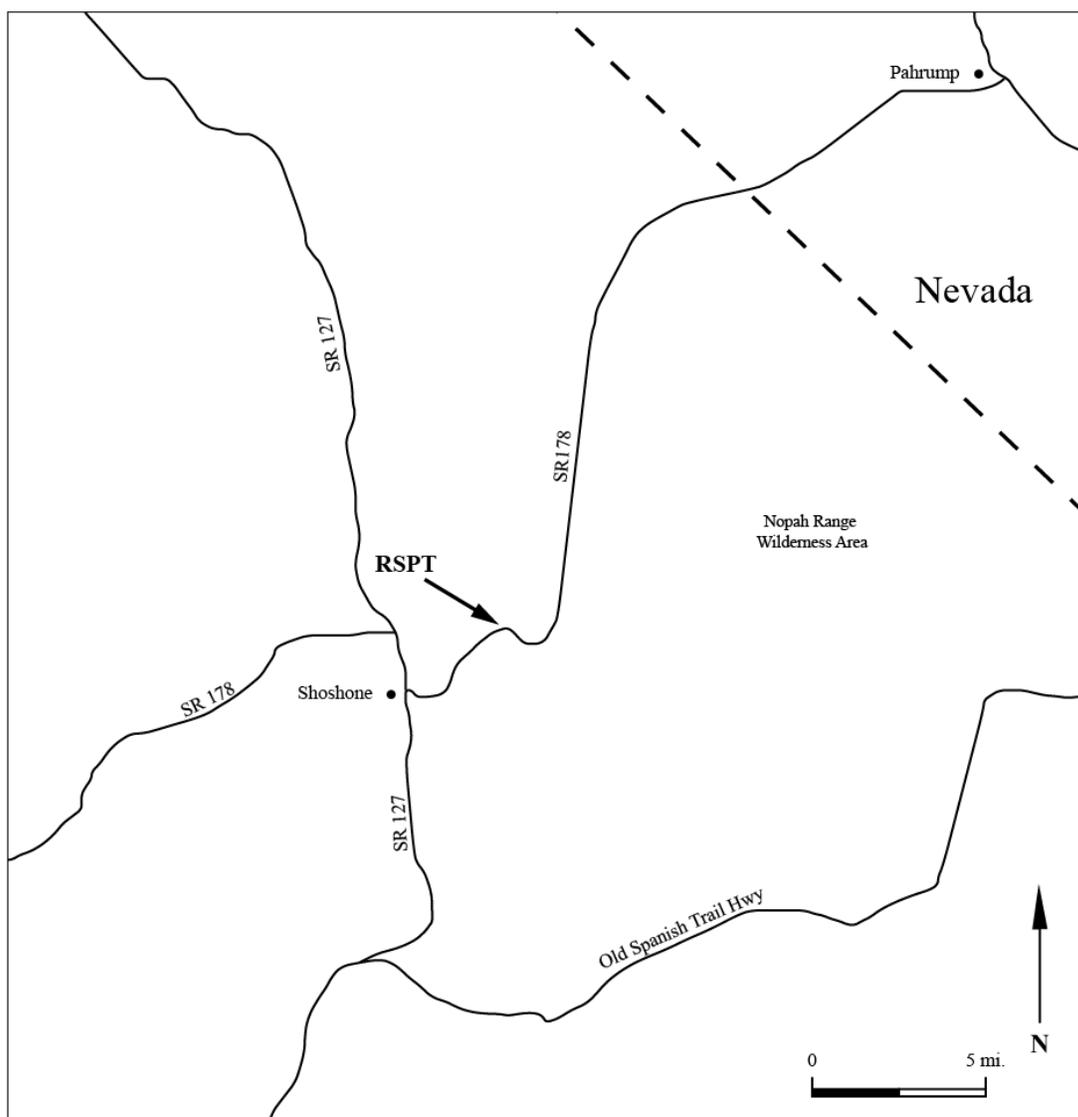
Figure 7. Location map of the roadcut along Hwy 178 where the Resting Springs Pass Tuff was studied.

Figure 8. Photo of the Resting Springs Pass tuff exposed in the roadcut along Hwy 178. The base of the unit is exposed in the lower right of the photo. Zones A, B, and C represent divisions of the outcrop made based on visual and textural differences readily noticeable at the outcrop scale. The dark band of obsidian through the middle of the deposit is the densely welded vitrophyre.
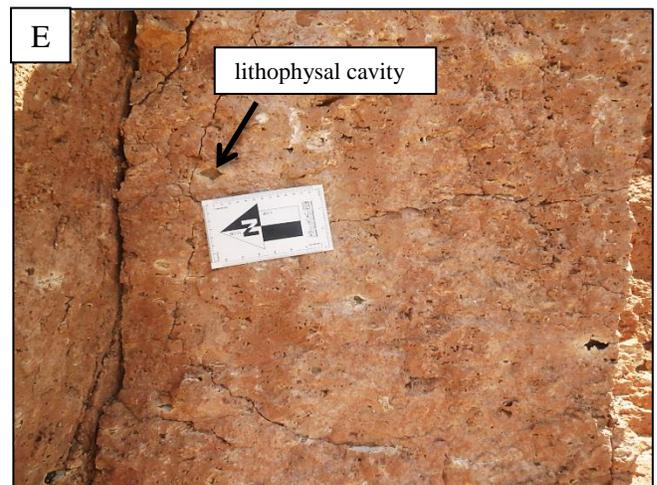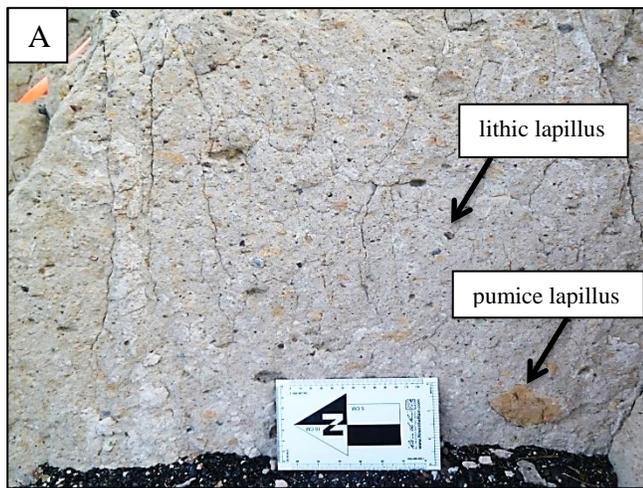
Figure 9. Photos highlighting the wide variation in appearance and texture of the Resting Springs Pass tuff. (A) Light-colored, non-welded lower portion of zone A. (B) Dark, densely welded upper portion of zone A. Key is 5.3 mm long. (C) Dark, densely welded zone C (vitrophyre). The white streaks are the vesicles in-filled with quartz, cristobalite, tridymite, and feldspar (Heydari, 1981). (D) Mottled lower portion of zone C. (E) Light-colored, densly-welded upper portion of zone C. Lithophysal cavities are extensive throughout this zone.
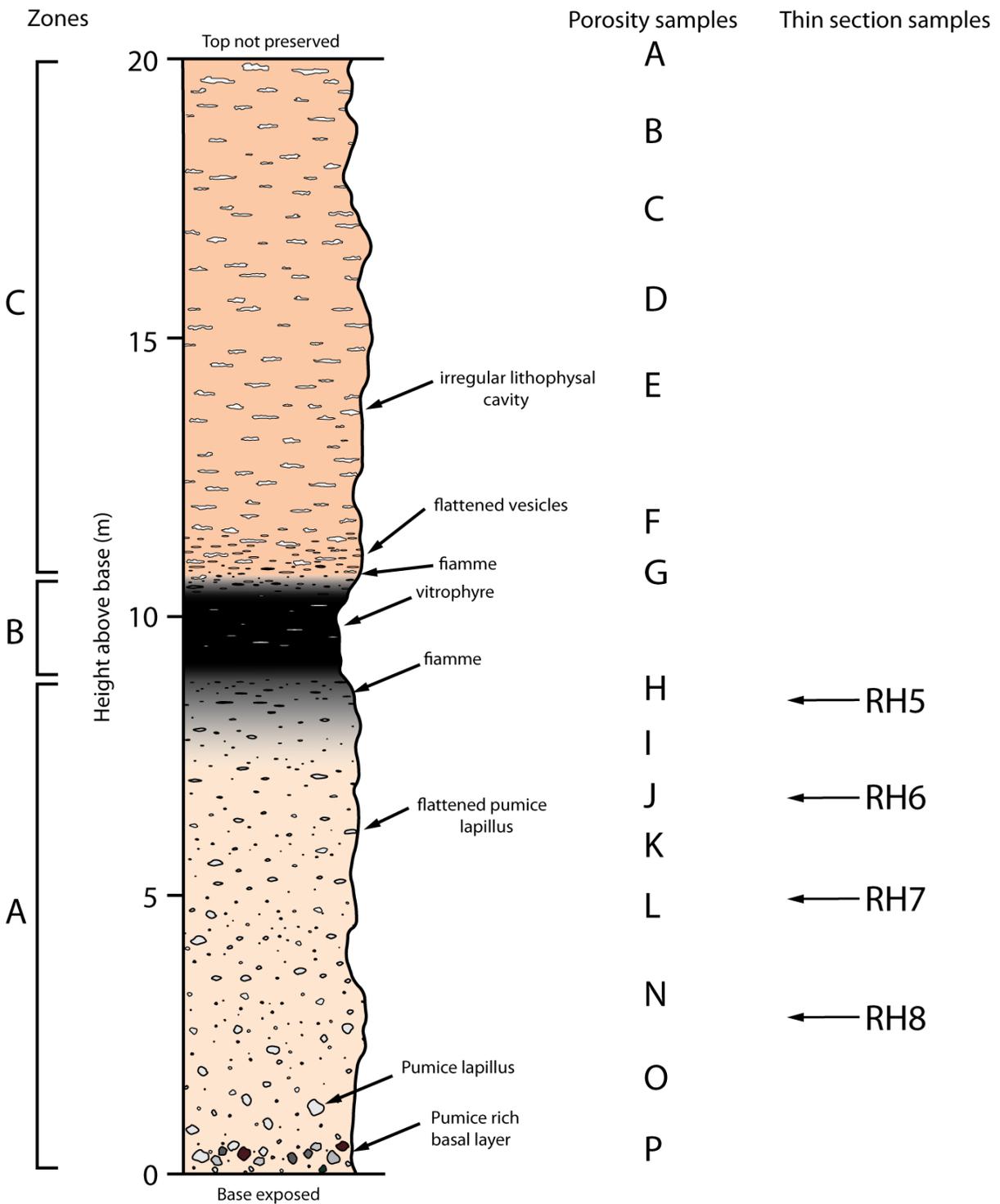
Figure 10. Stratigraphic column of the Resting Springs Pass tuff as it appears in the Hwy 178 roadcut. The RSPT has been divided into three informal zones: A, B, and C. Height locations for thin section and porosity samples indicated to the right.
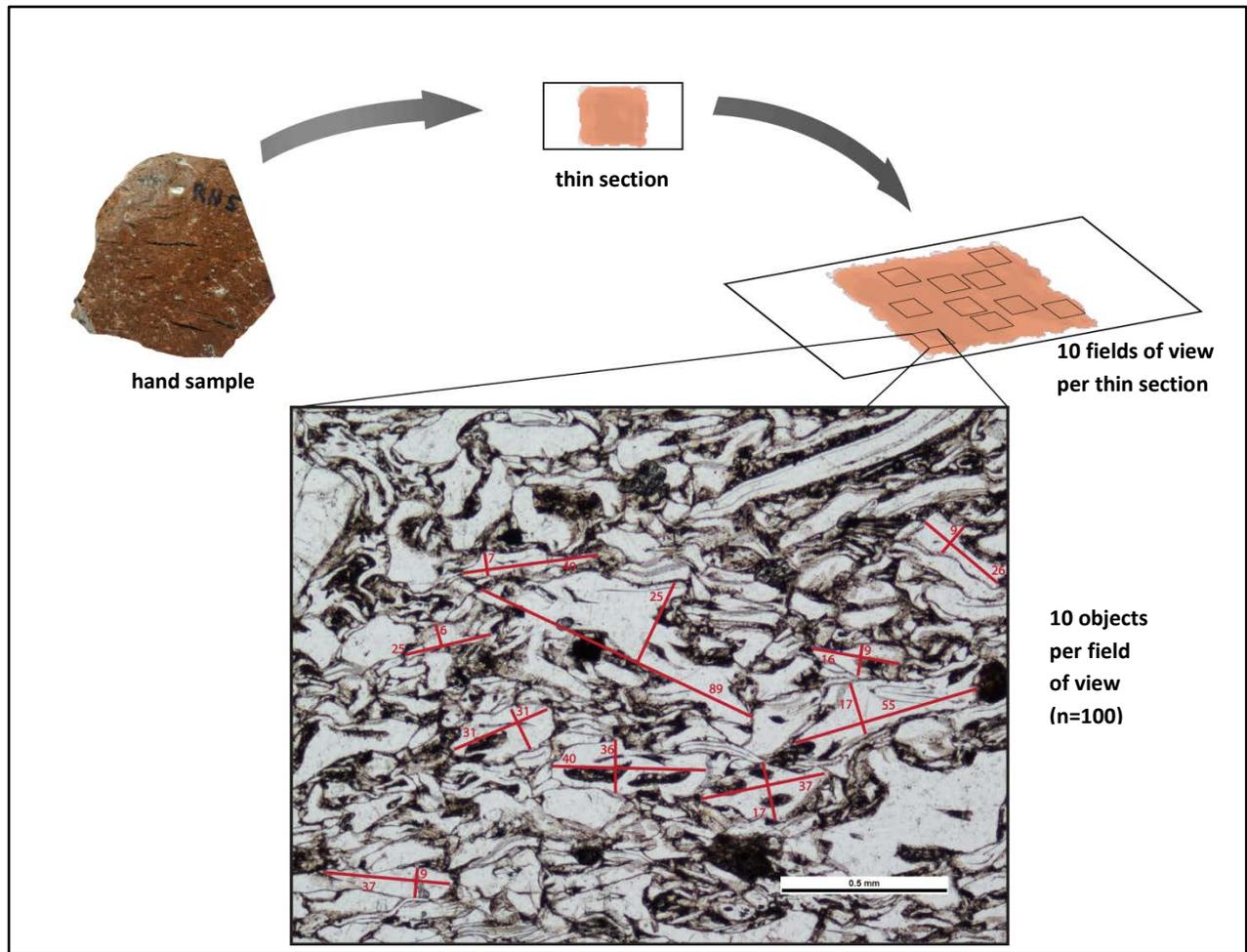
Figure 11. Illustrated method for measuring strain in ash matrix. A hand sample is collected from outcrop and made into thin section. Ten photographs are taken from different locations within the thin section. Next, ten 2D strain measurements are taken from each photo. The total number of strain measurements from each sample is 100.

Figure 12. Photo of the samples used to determine porosity for various locations within the RSPT (powdered samples O and P not shown). Cylindrical samples measure approximately 1 inch (25mm) in diameter. Samples I and N are cuboid shaped.
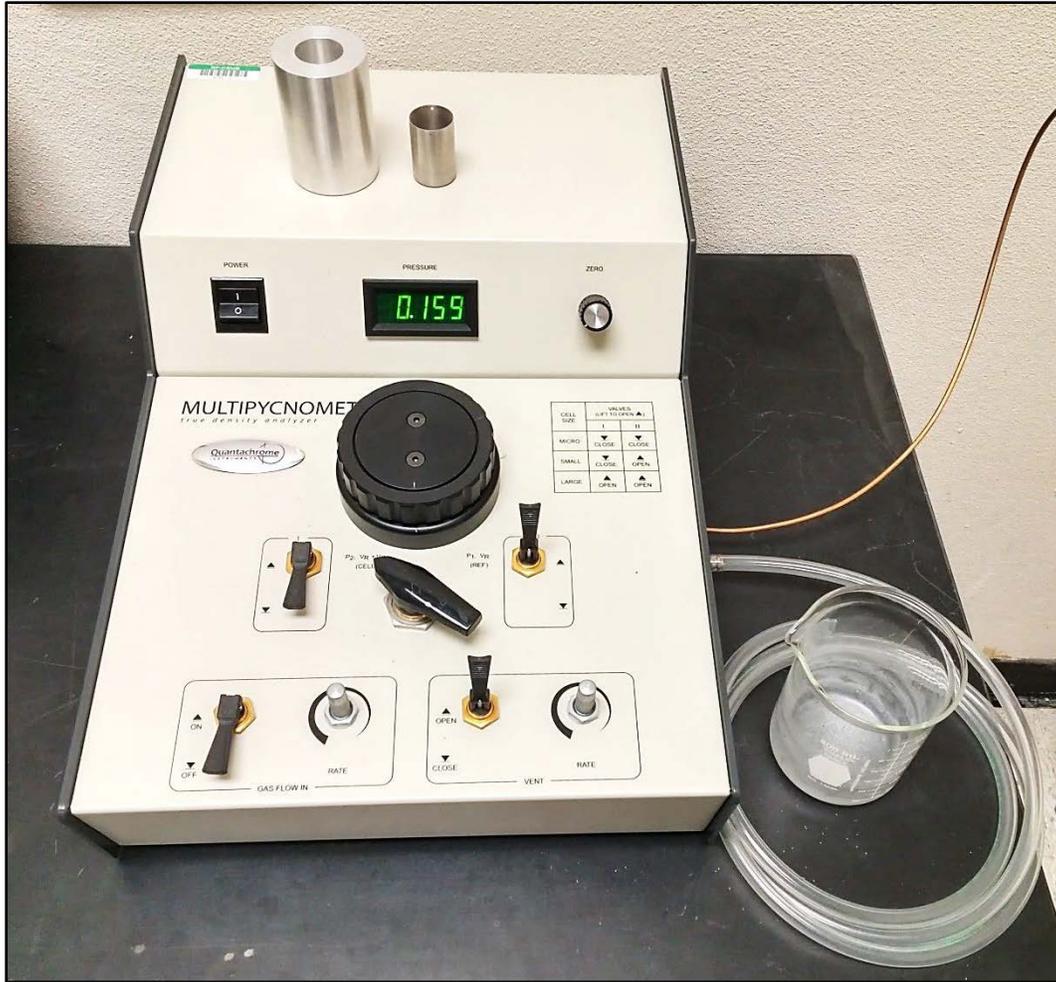
Figure 13. Photo of the Quatachrome Multipycnometer used to determine porosity from core and powdered samples.
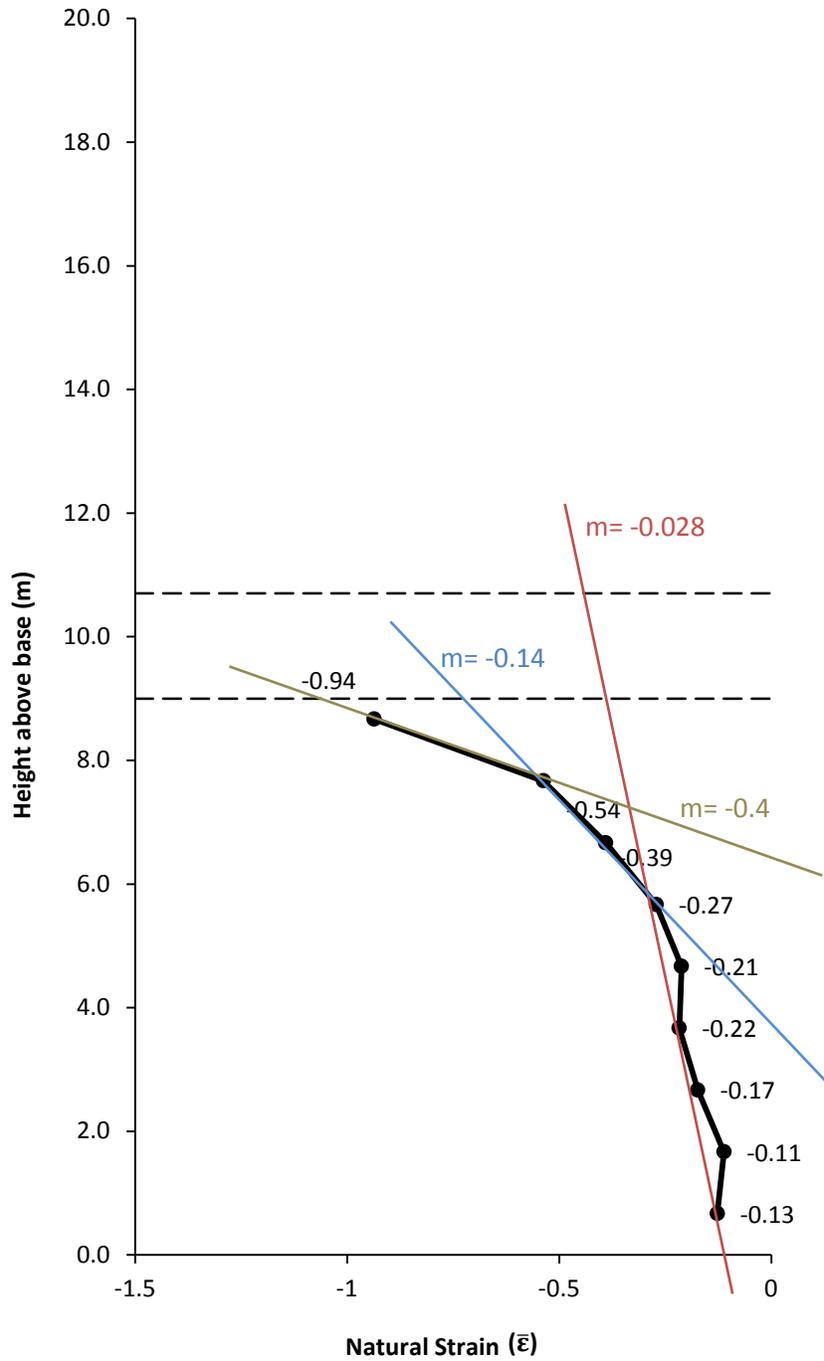
Figure 14. Natural strain log through Zone A of the Resting Springs Pass Tuff. Strain measurements are gathered from the pumice and fiamme clasts. Colored lines illustrate changing strain gradients.
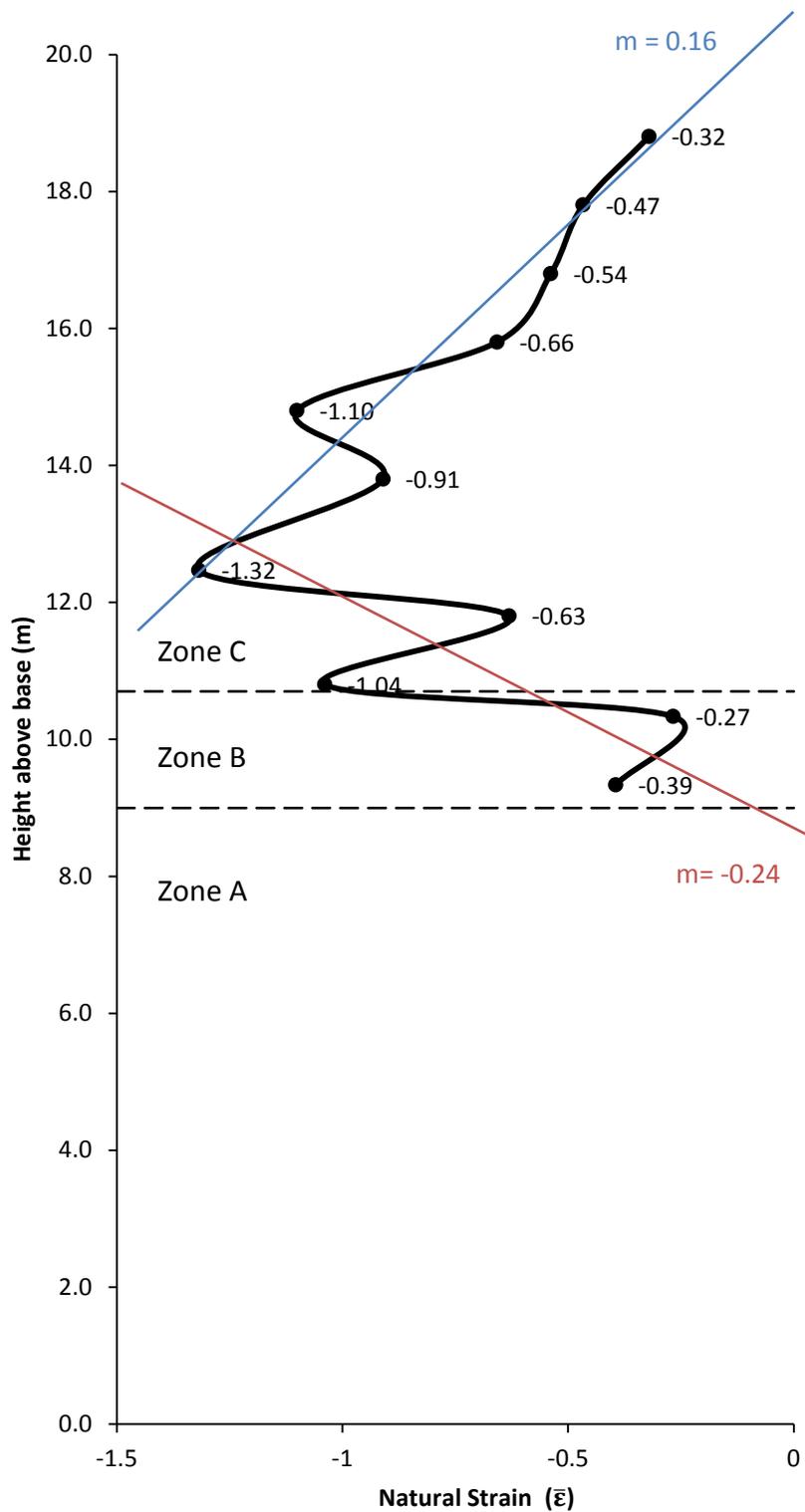
Figure 15. Natural strain log through the Resting Springs Pass tuff from data gathered from macroscopic voids. Colored lines illustrate changing strain gradients.
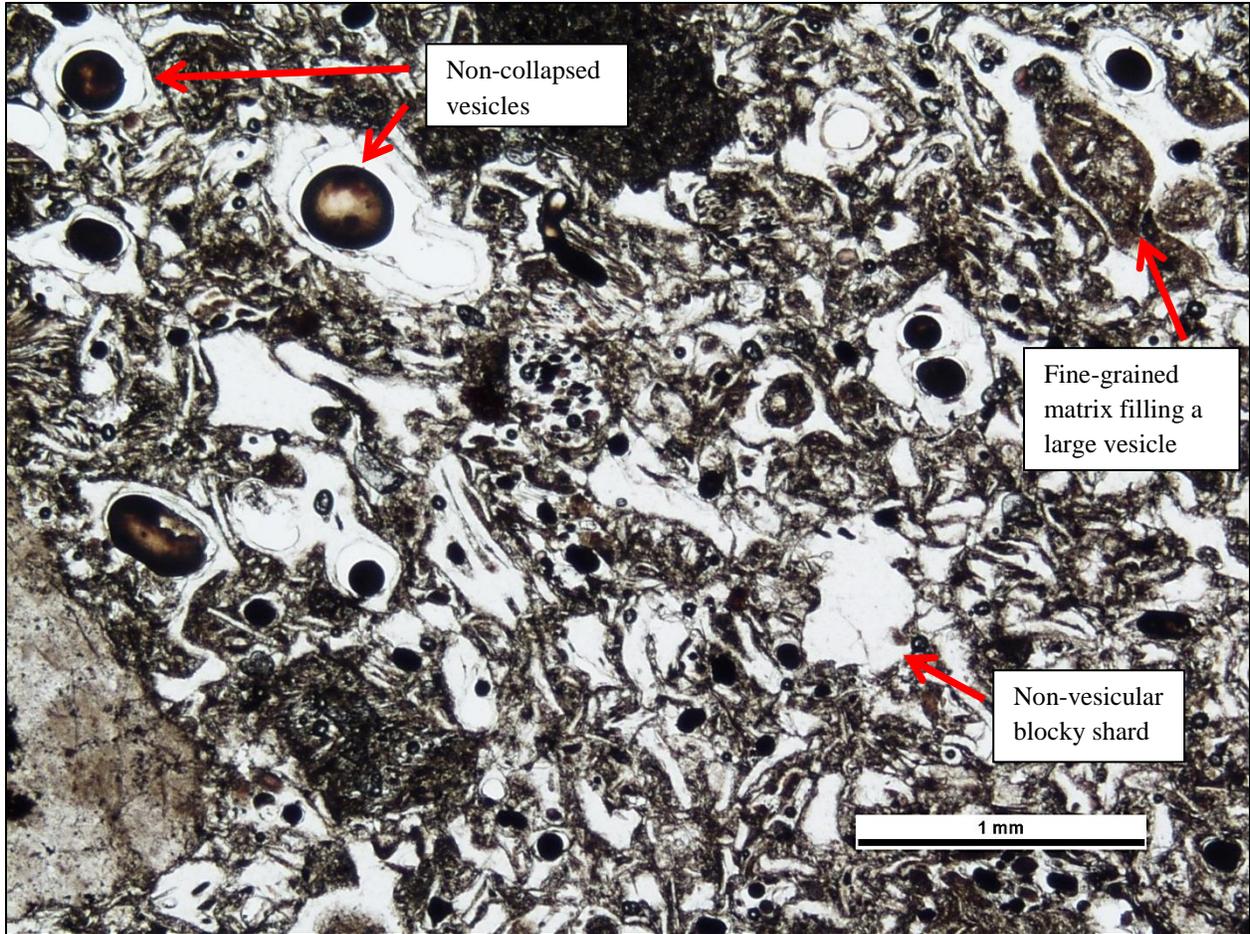
Figure 16A. Photo of thin section RH8 at 20x magnification, PPL. Note the wide range of vesicularities amongst the different clasts seen in this sample.
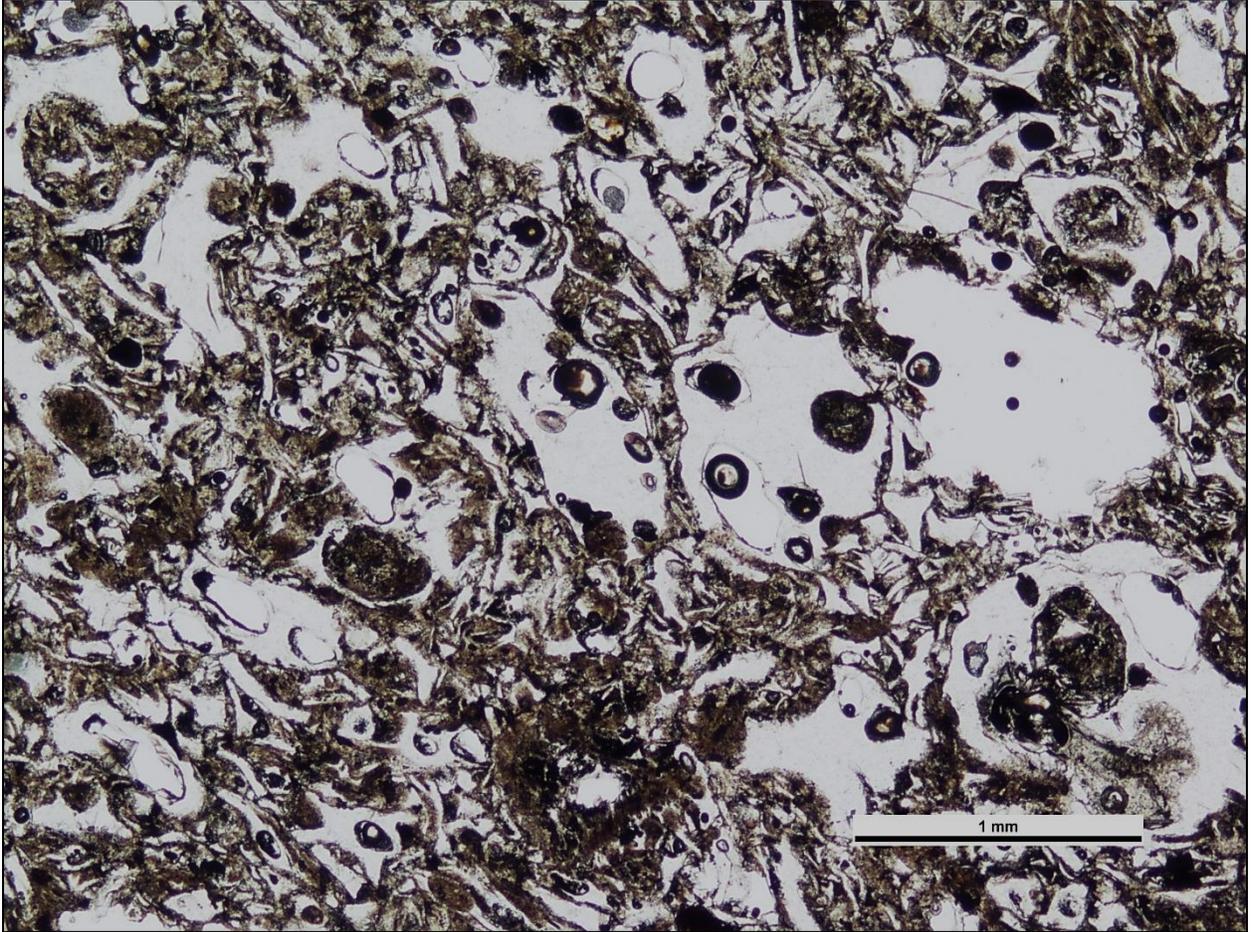
Figure 16B. Photo of thin section RH7 at 20x magnification, PPL.
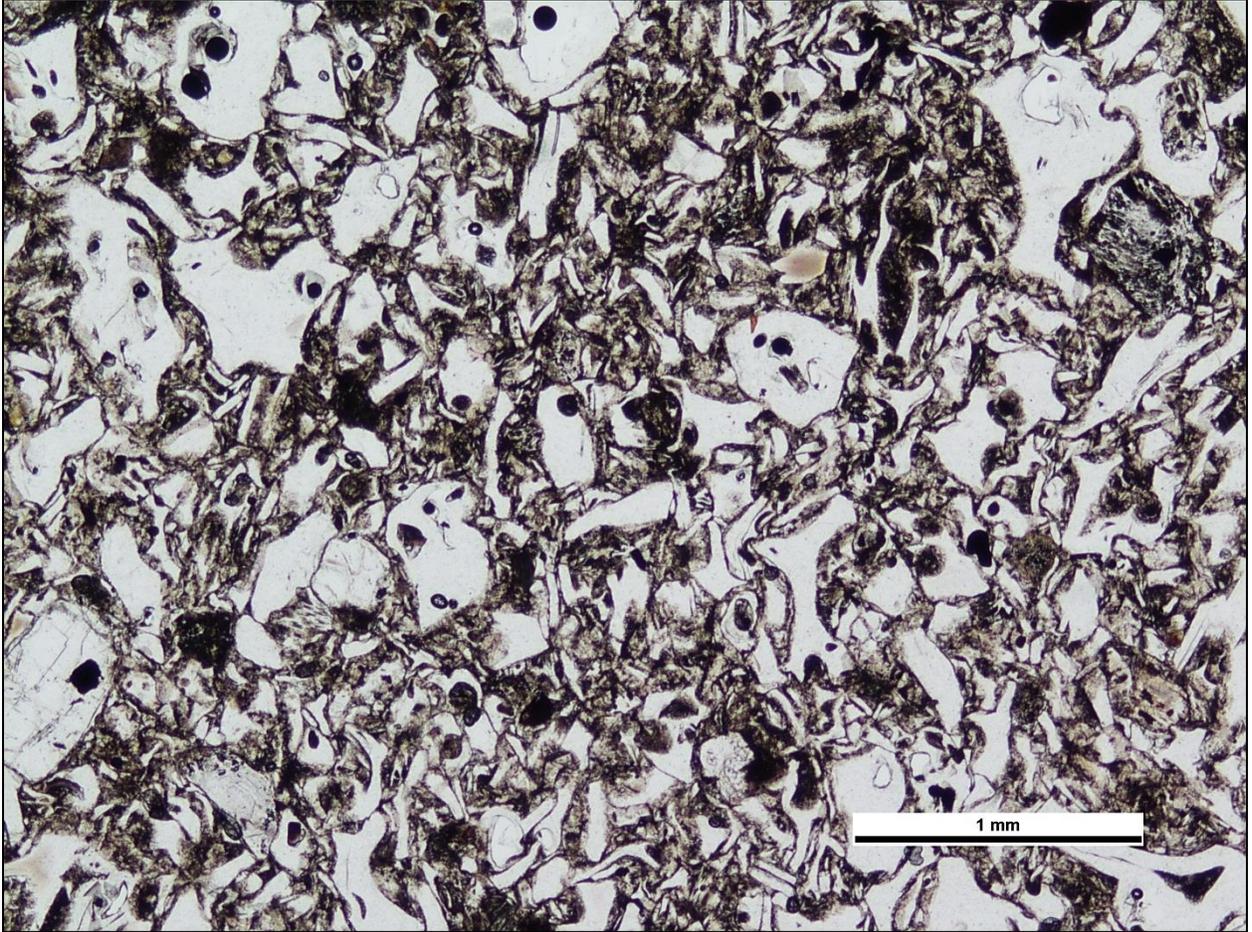
Figure 16C. Photo of thin section RH6 at 20x magnification, PPL.
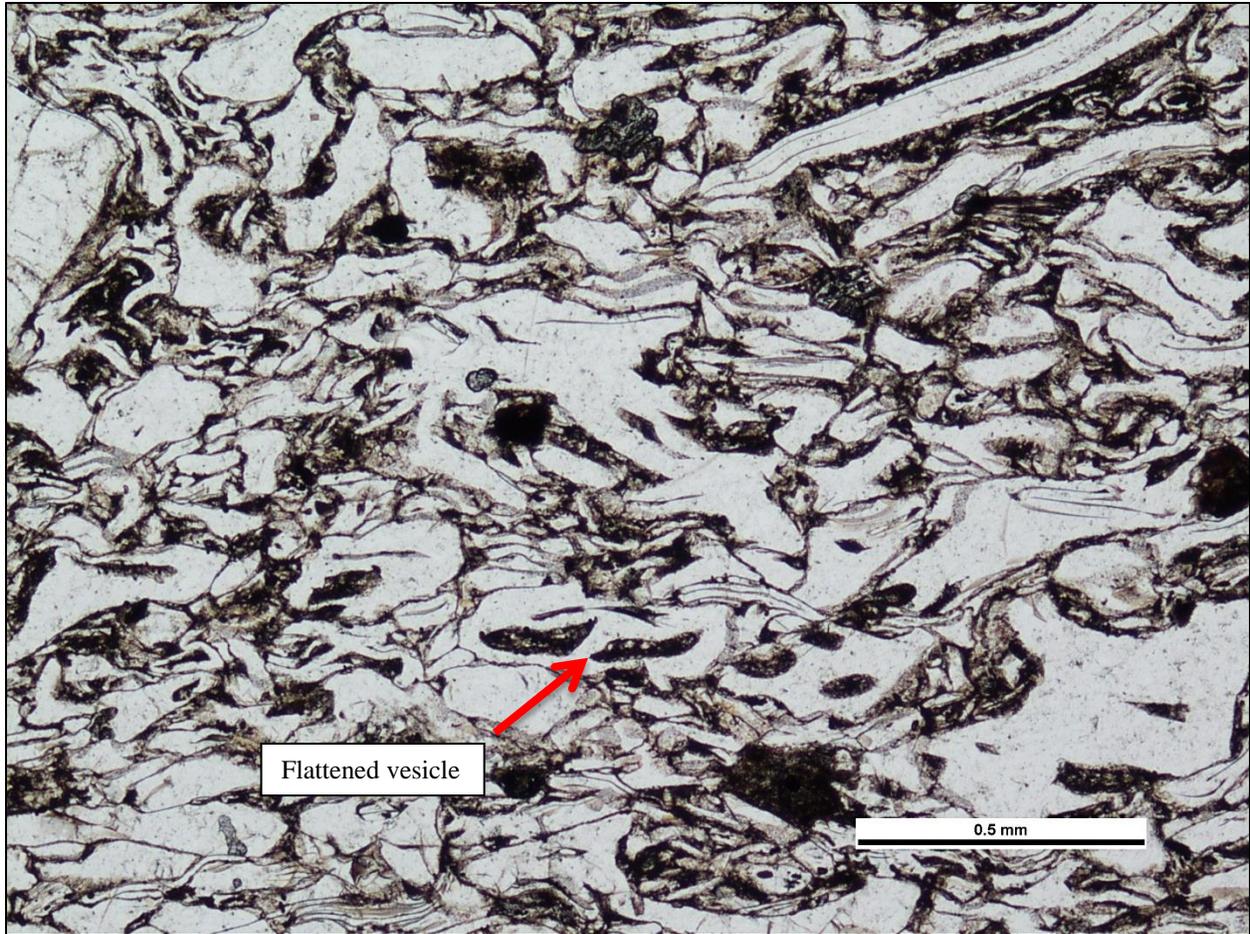
Figure 16D. Photo of thin section RH5 at 40x magnification, PPL. Note the strong preferred orientation (eutaxitic foliation) amongst the readily visible ash shards. Flattened vesicles can still be seen in some of the shards.
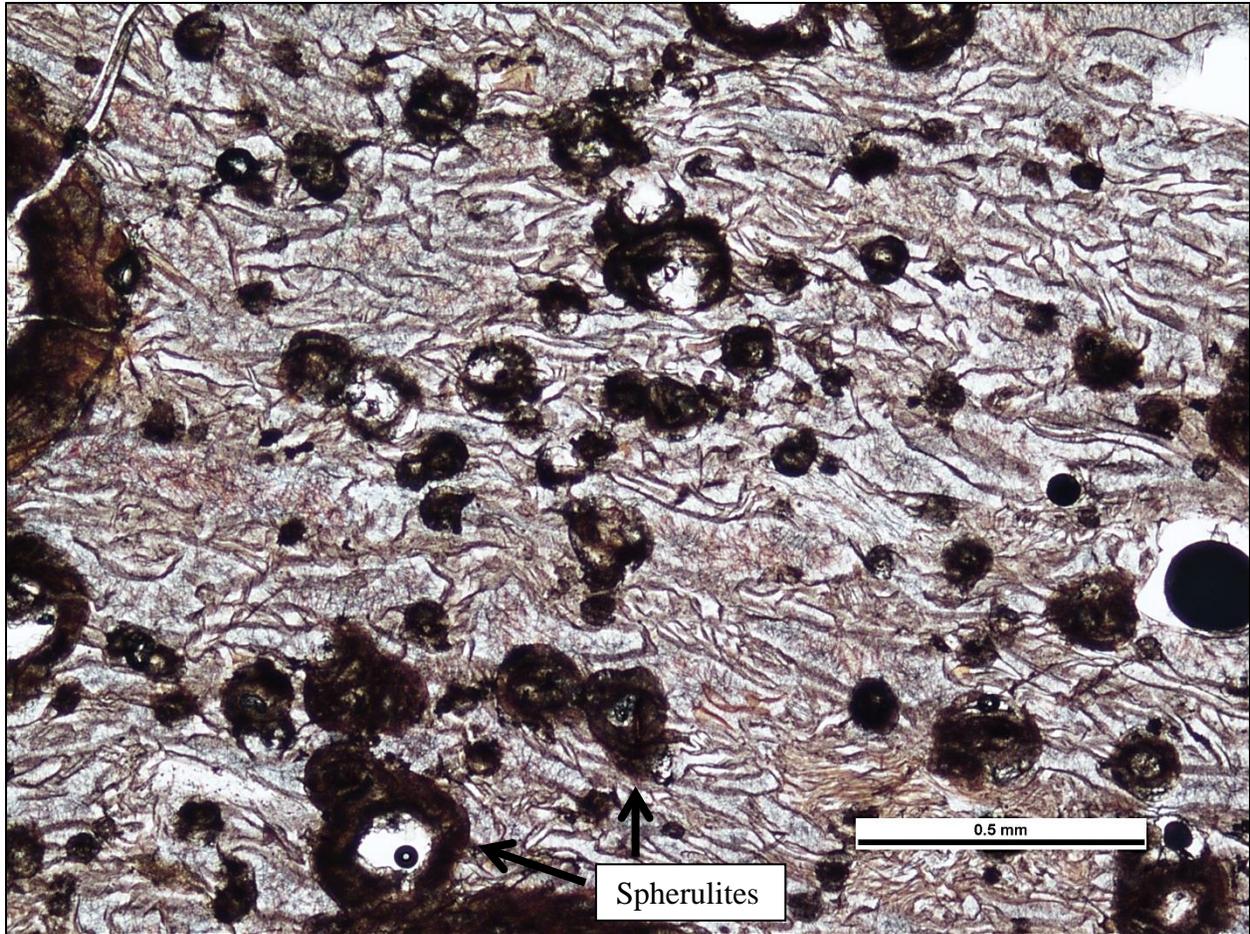
Figure 16E. Photo of thin section RH4 at 40x magnification, PPL. Note the strong eutaxitic foliation oriented from the upper left to the lower right, as well as the general absence of vesicles.
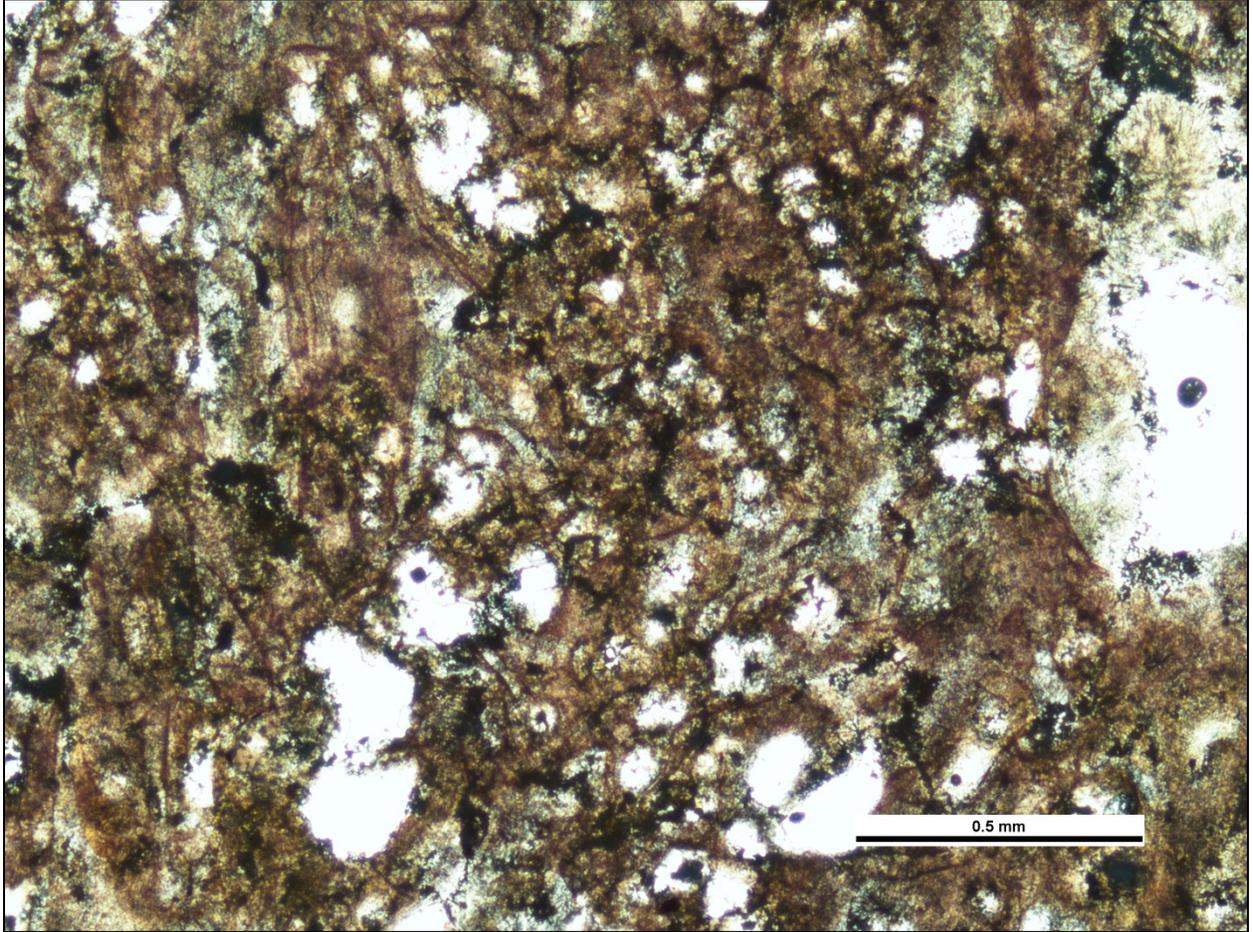
Figure 16F. Photo of thin section RH3 at 40x magnification, PPL. Pervasive mottle-overprinting has obscured all original grain shapes.
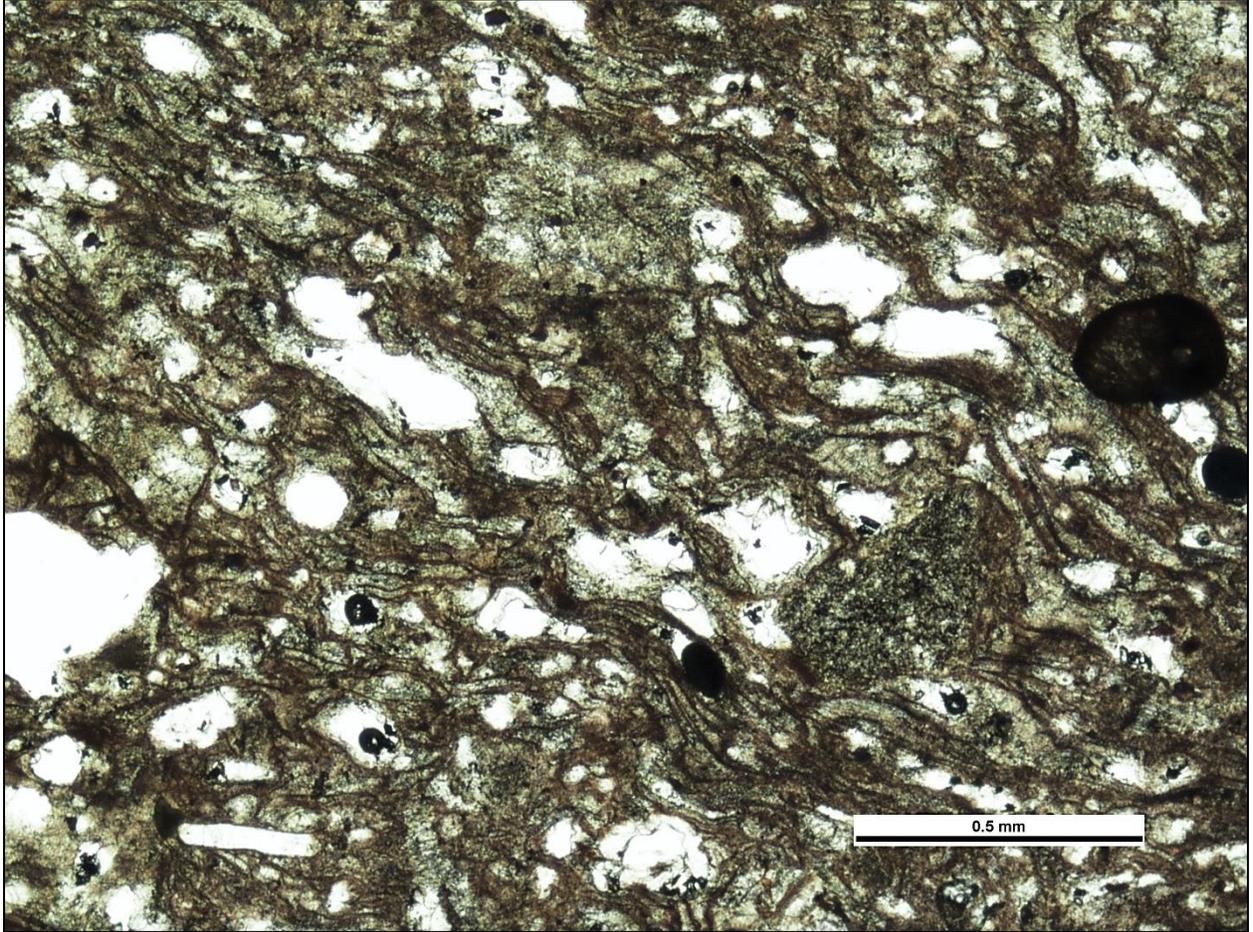
Figure 16G. Photo of thin section RH2 at 40x magnification, PPL. Note dark wispy lines are ash shards whose boundaries have become obscured due to devitrification.
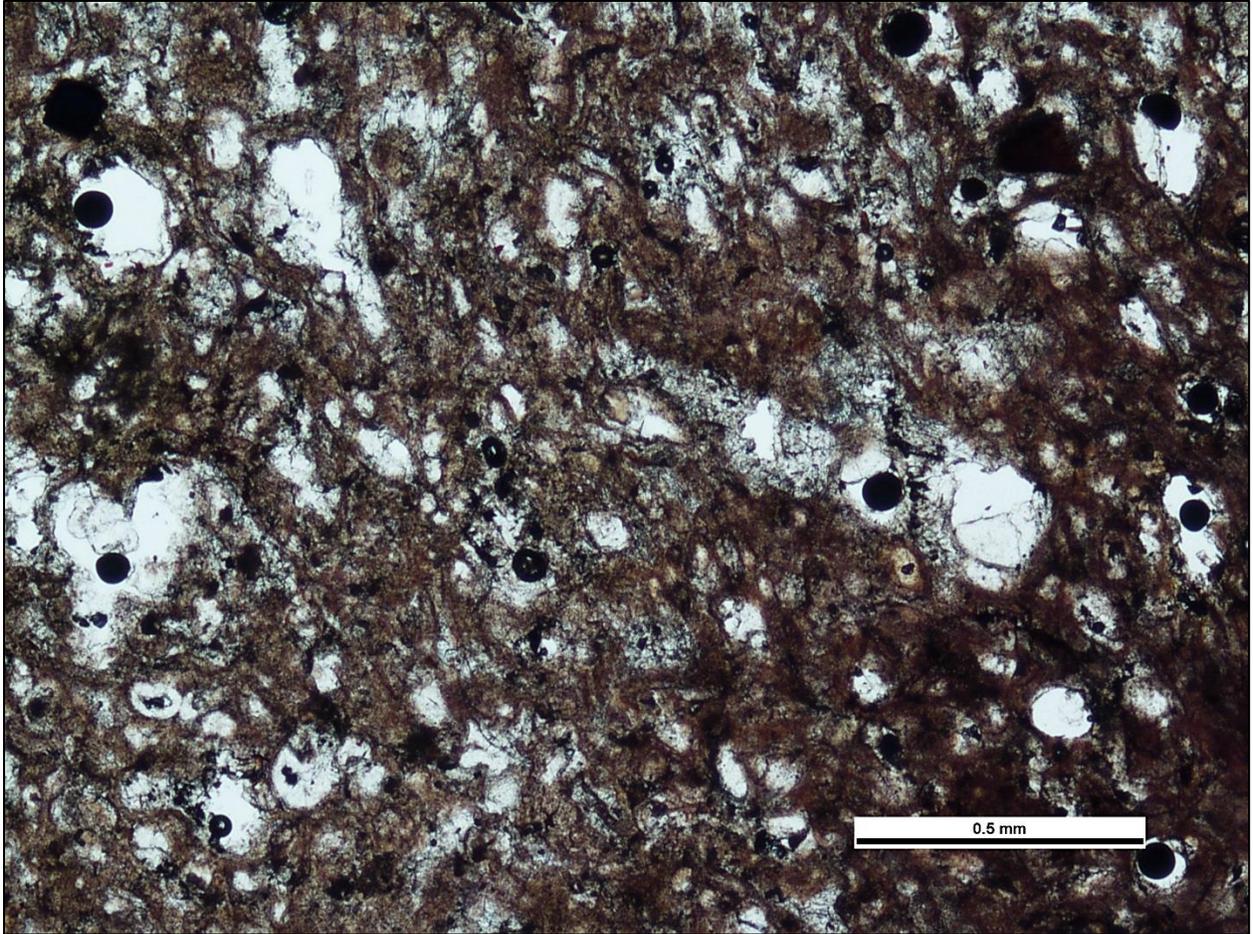
Figure 16H. Photo of thin section RH1 at 40x magnification, PPL. Pervasive mottling makes individual shard boundaries indistinguishable.
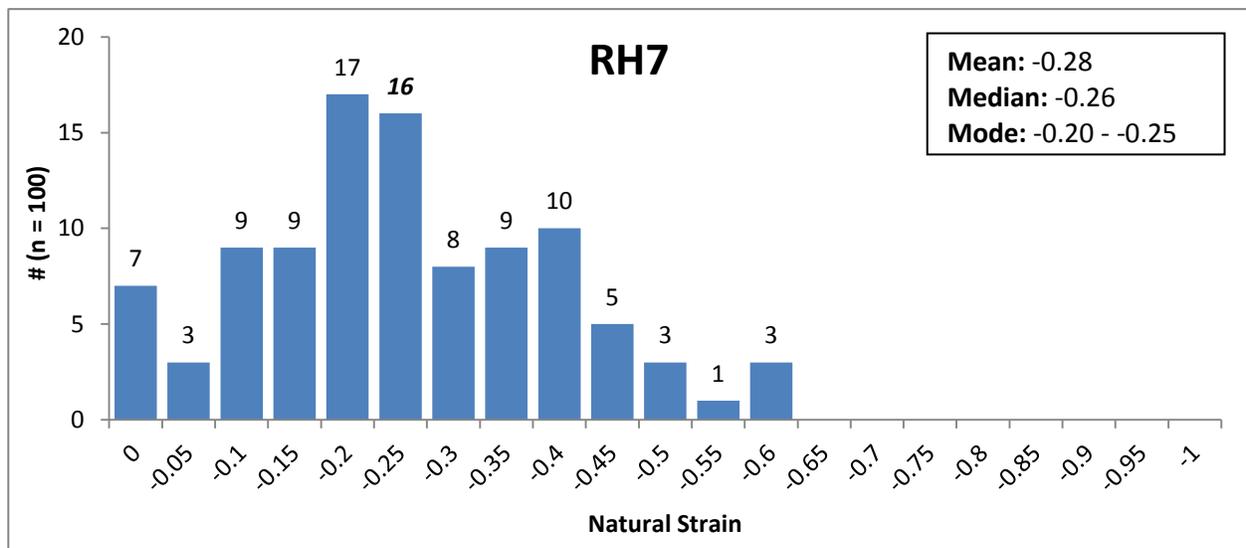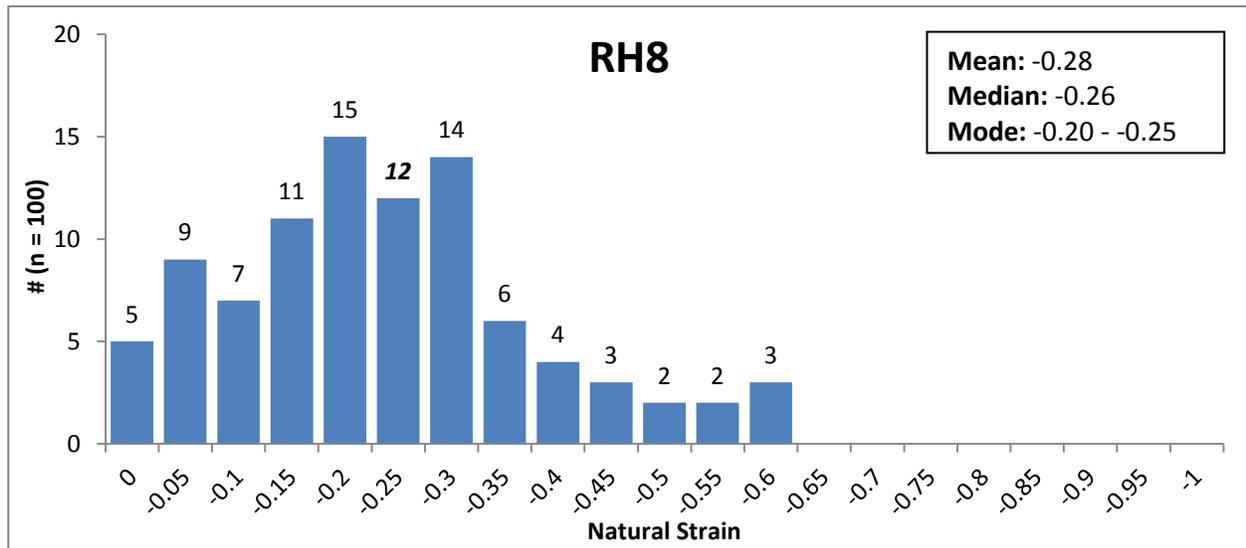
Figure 17a. Histograms showing strain value statistics for samples RH8 and RH7. Modal values are a range.
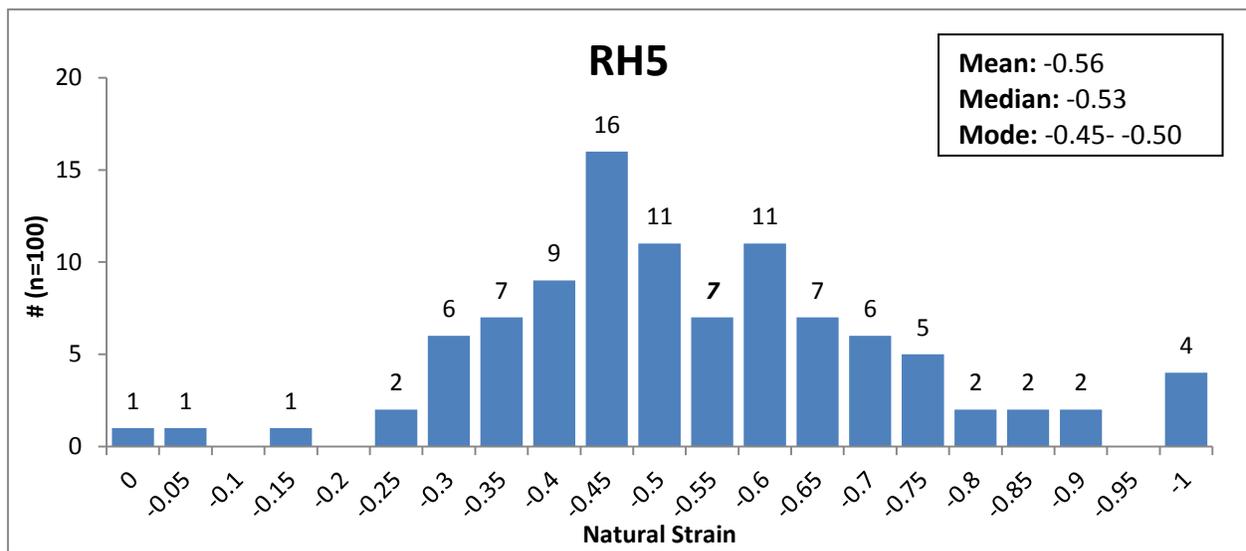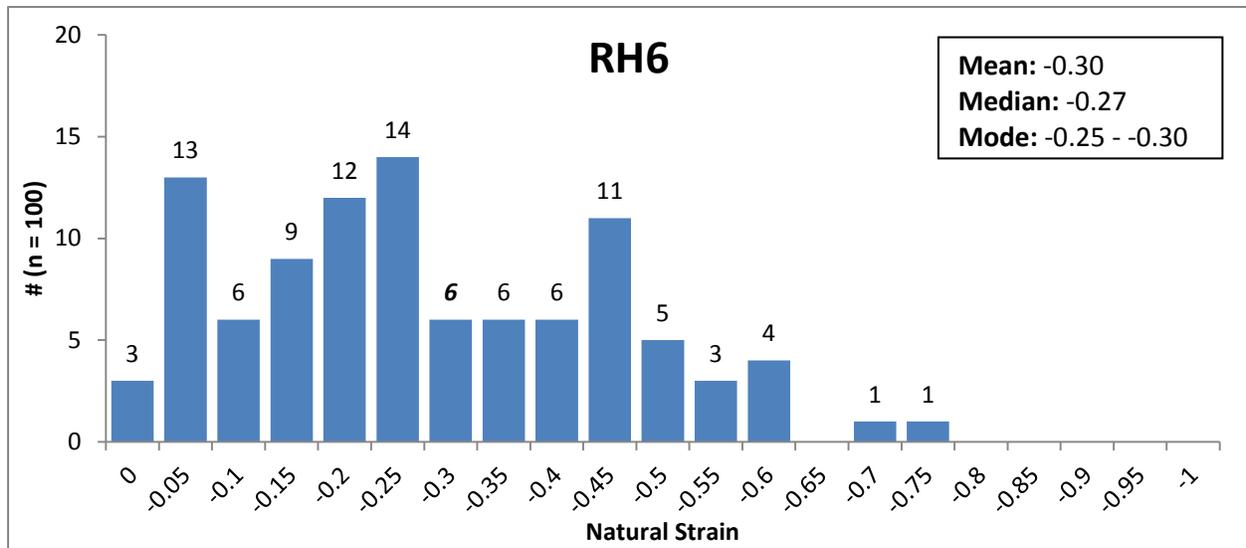
Figure 17b. Histograms showing strain value statistics for samples RH6 and RH5. Modal values are a range.
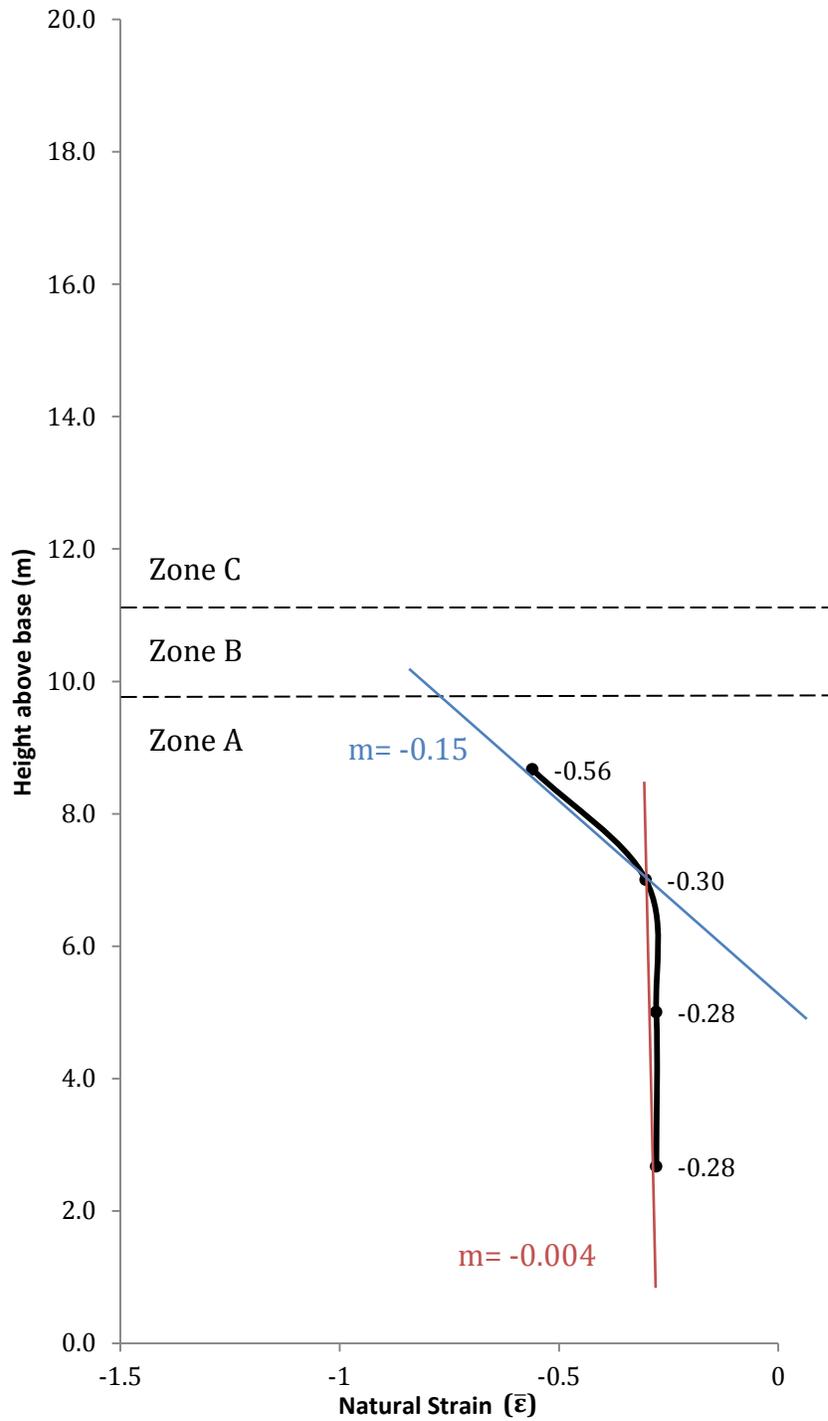
Figure 18. Graph showing average natural strain values from ash matrix. Colored lines illustrate changing strain gradients.
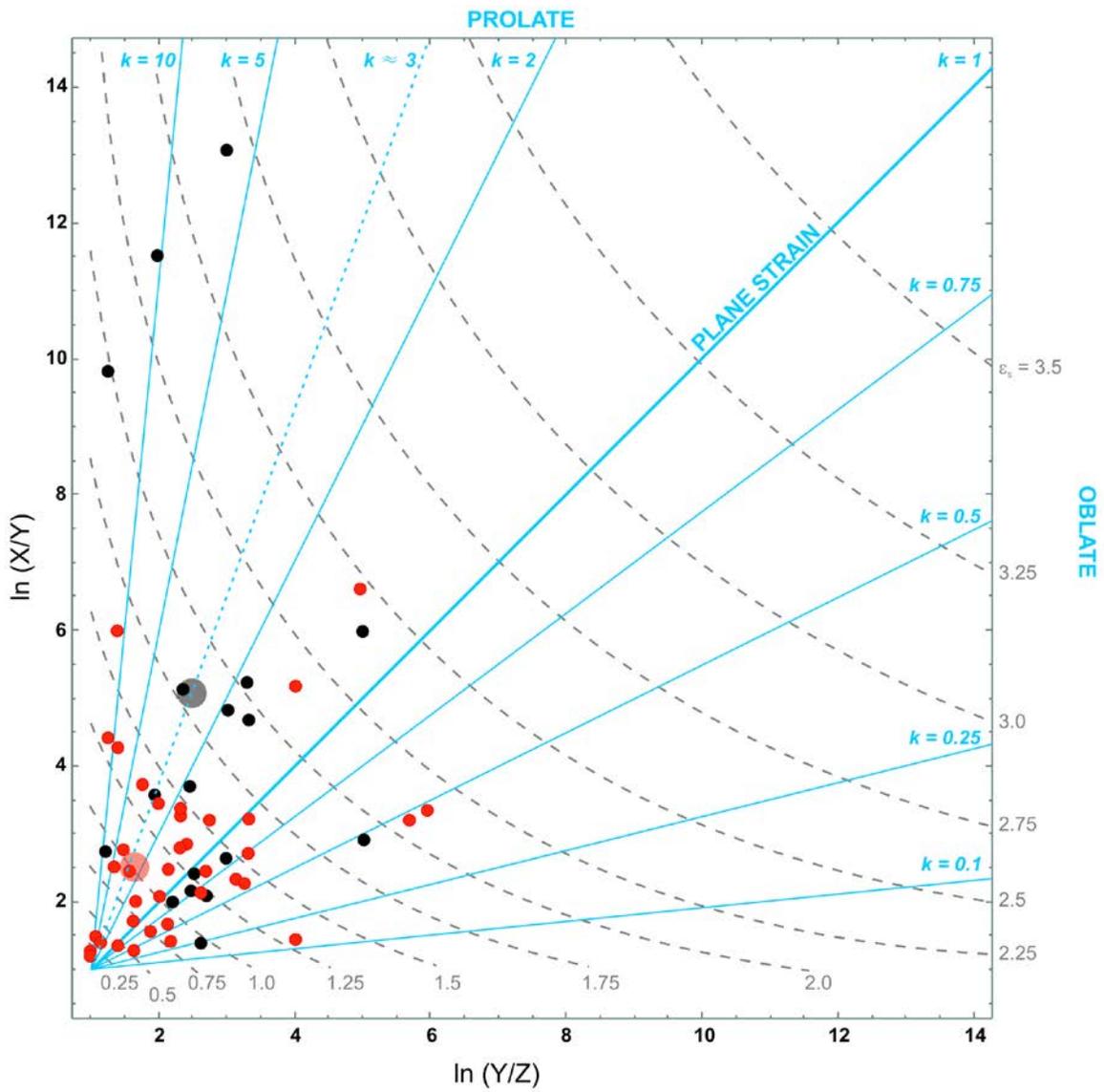
**Figure 19.** Three dimensional strain data from zone B (black dots) and zone C (orange dots) plotted on a Flinn diagram. The large grey and orange dots represent average values. The data indicates that the average shape of macroscopic voids in both zones A and B is prolate.
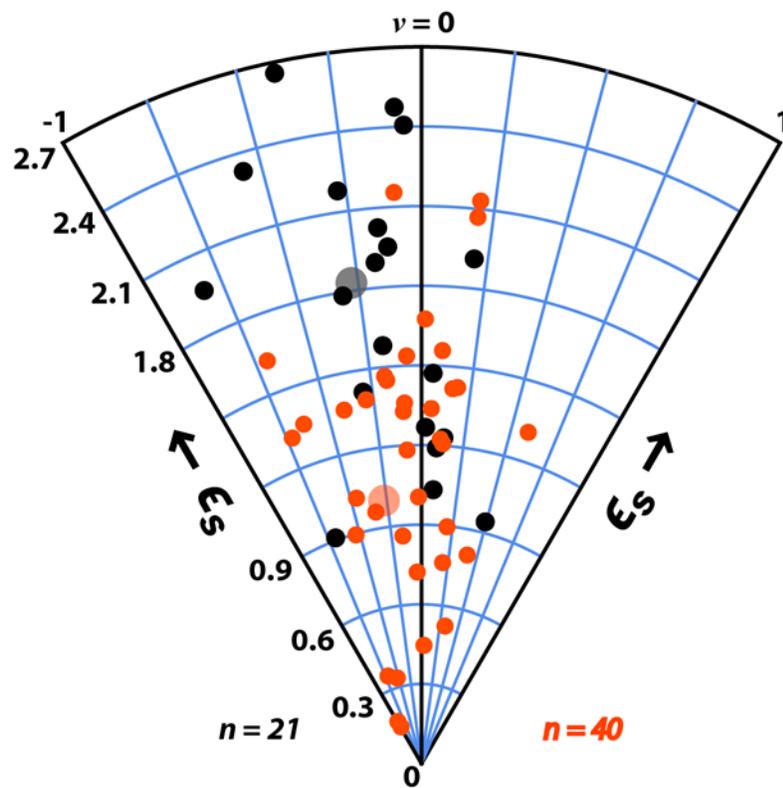
Figure 20. Three-dimensional strain data from zone B (black dots) and zone C (orange dots) plotted on a Hsu diagram. E_s indicates total strain. Lode parameter values of -1 and 1 indicate a pure prolate and oblate shapes respectively.
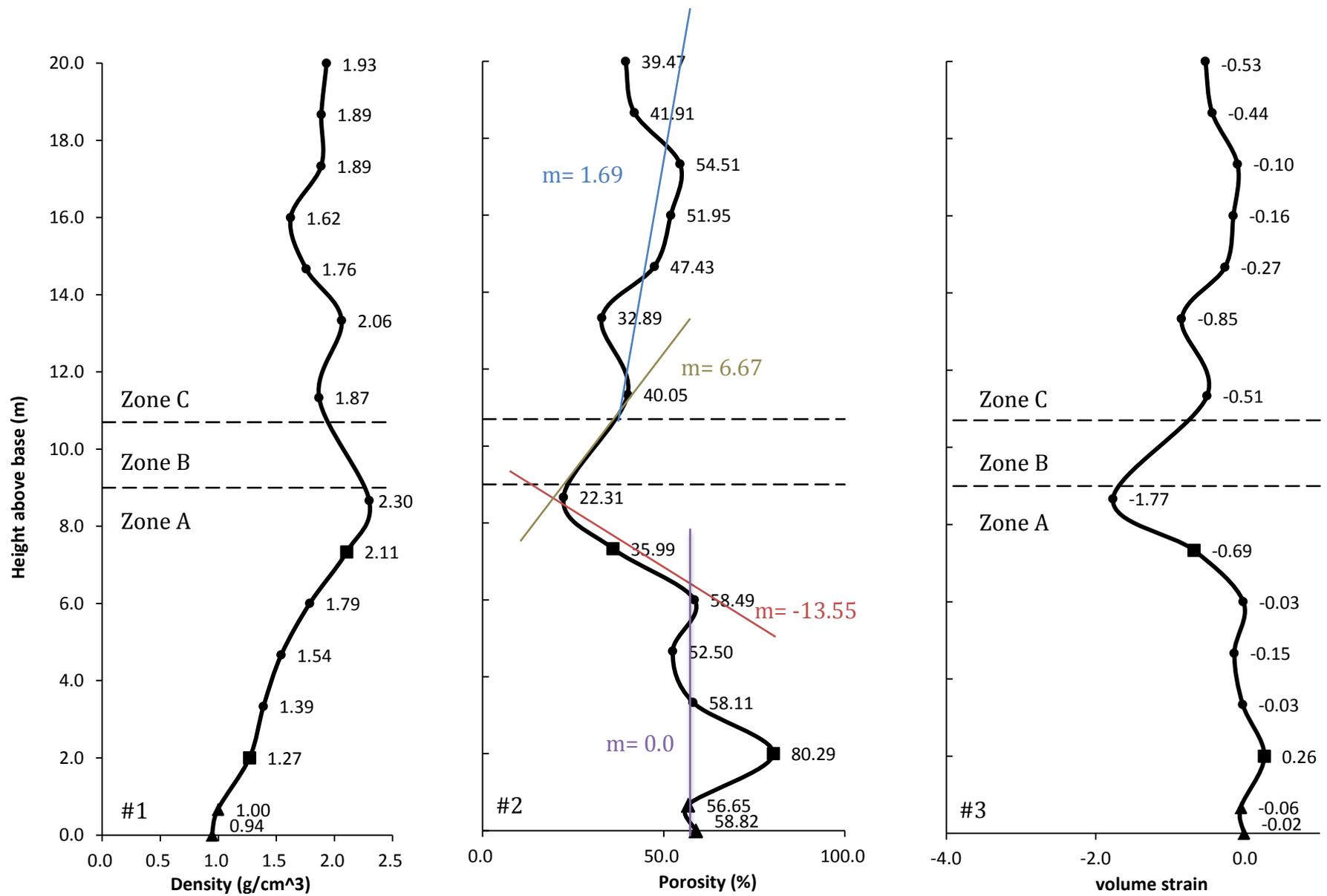
Figure 21. Density , porosity, and volume strain logs for the Resting Springs Pass tuff. Triangular and square data points indicate samples that were crumbled and cut into cuboids respectively.
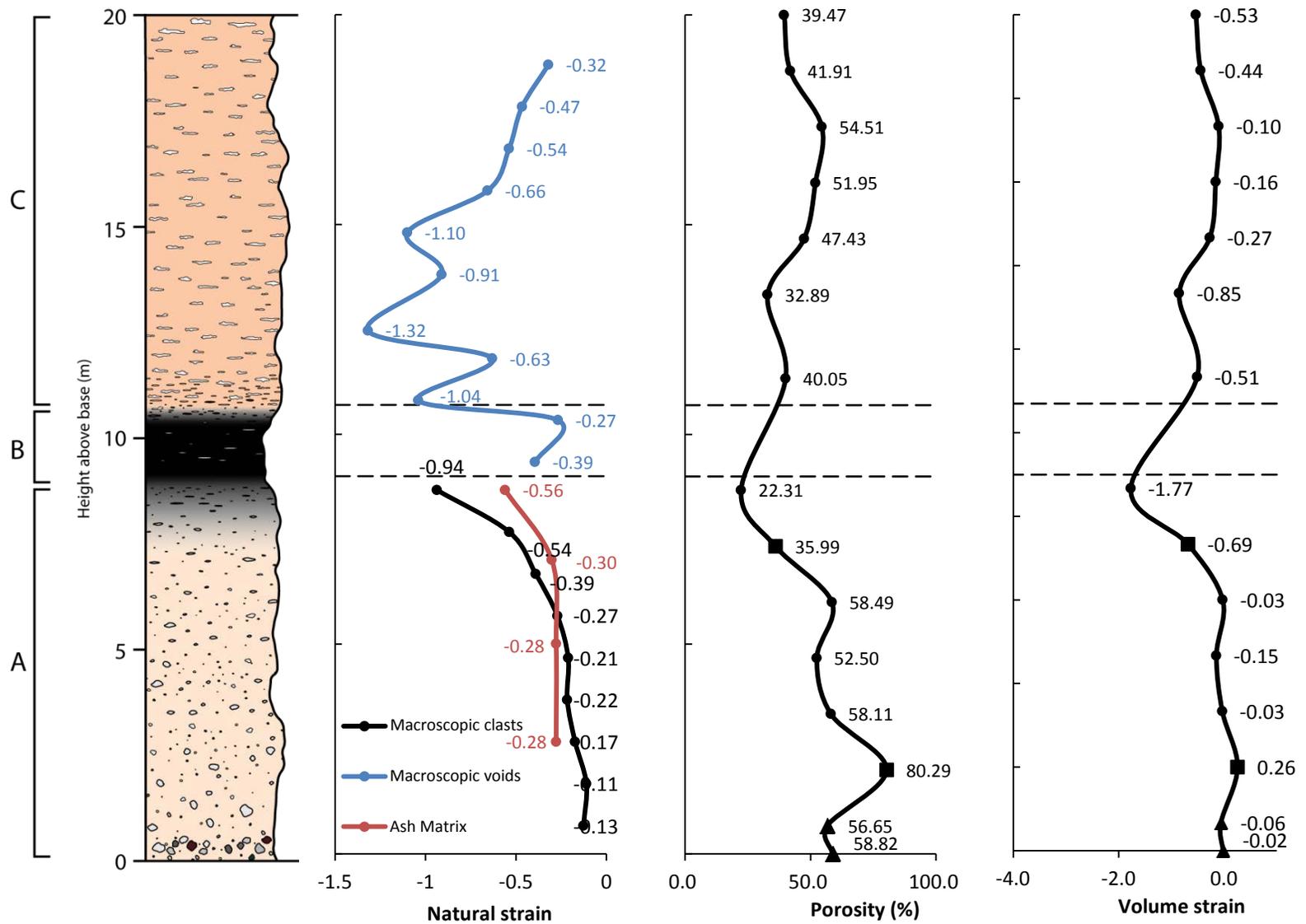
Figure 22. Side-by-side comparison of stratigraphic section, natural strain, porosity, and volume strain logs from the Resting Springs Pass tuff. The natural strain log is a composite of three different datasets that are identified by their different colors.
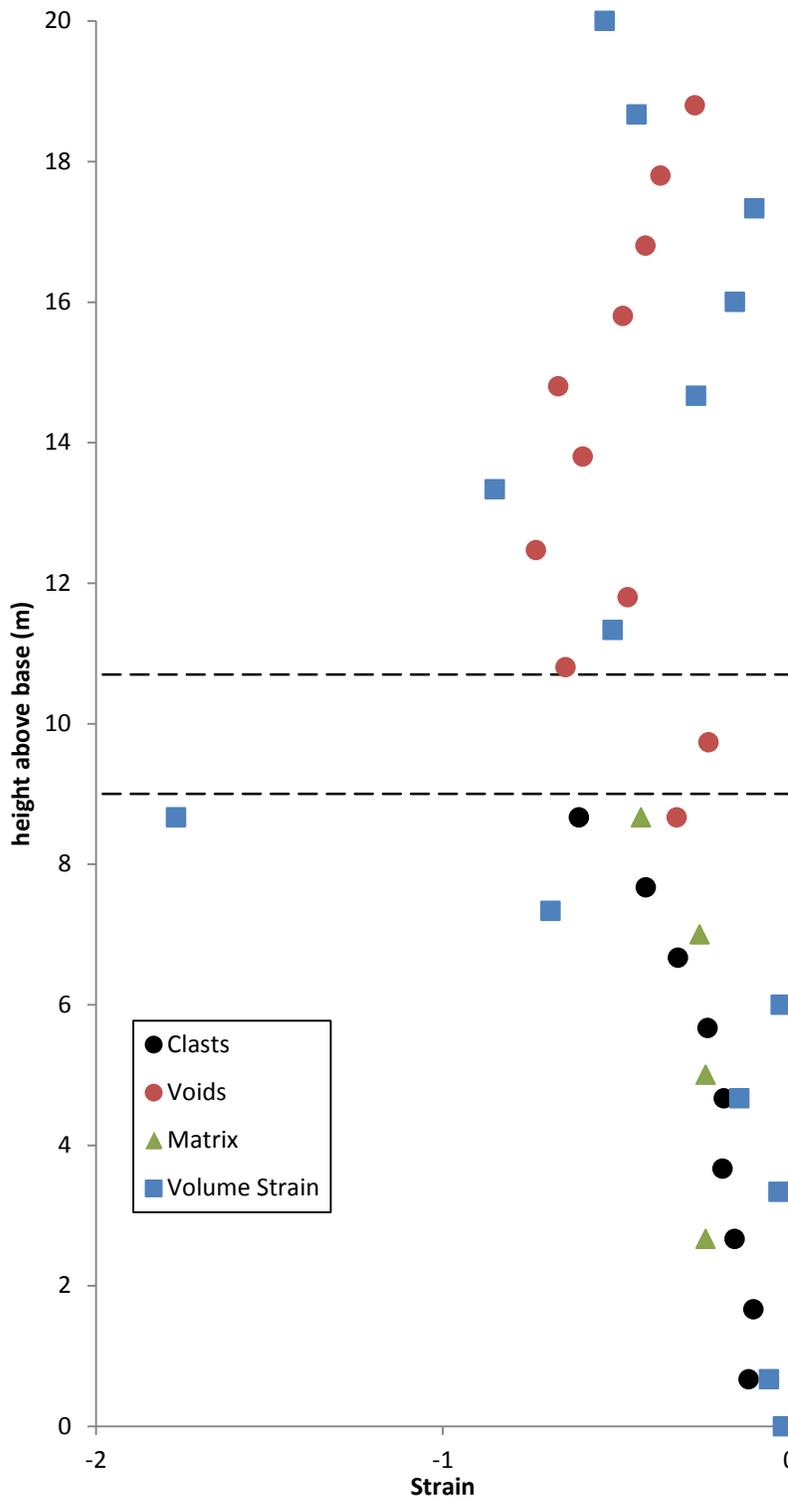
Figure 23. Graph showing comparison of strain values
gathered from different petrophysical and petrofabric datasets.
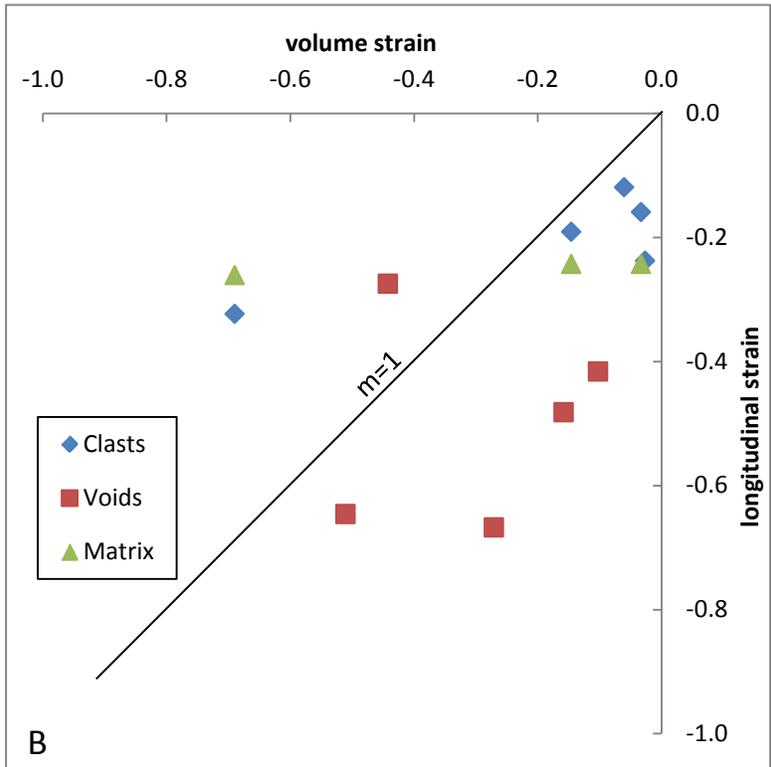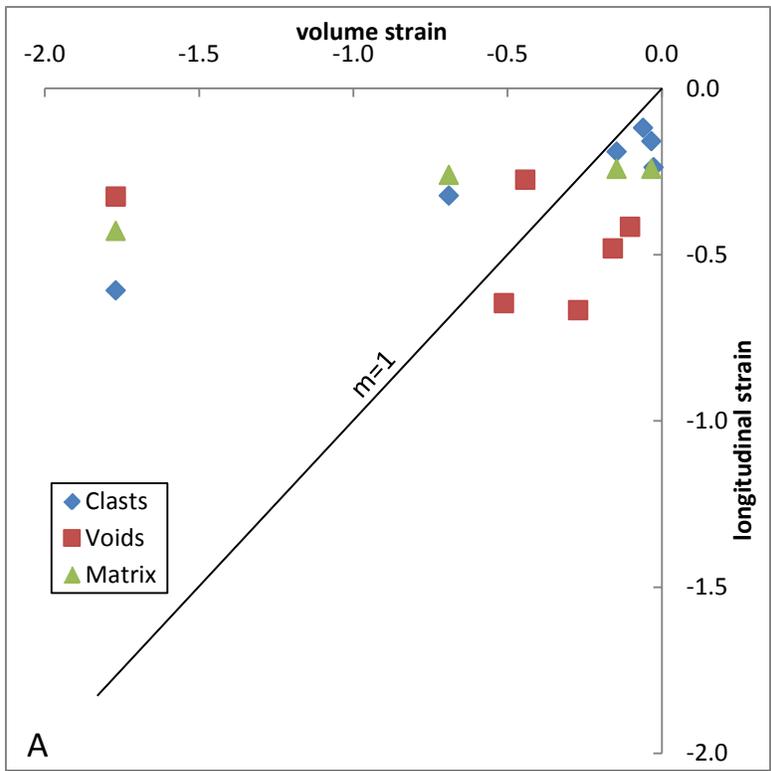
Figure 24. Comparison of volume strain from three different data sets. Figure B omits data in and closest zone B.